

# The CH<sub>4</sub> cycles on Pluto over seasonal and astronomical timescales

T. Bertrand<sup>a</sup>, F. Forget<sup>b</sup>, O.M. Umurhan<sup>a</sup>, J.M. Moore<sup>a</sup>,  
 L.A. Young<sup>c</sup>, S. Protopapa<sup>c</sup>, W.M. Grundy<sup>d</sup>, B. Schmitt<sup>e</sup>,  
 R.D. Dhingra<sup>f</sup>, R.P. Binzel<sup>g</sup>, A.M. Earle<sup>g</sup>, D.P. Cruikshank<sup>a</sup>,  
 S.A. Stern<sup>c</sup>, H.A. Weaver<sup>h</sup>, K. Ennico<sup>a</sup>, C.B. Olkin<sup>c</sup>,  
 the New Horizons Science Team,

<sup>a</sup>*National Aeronautics and Space Administration (NASA), Ames Research Center,  
 Space Science Division, Moffett Field, CA 94035, United States*

<sup>b</sup>*Laboratoire de Météorologie Dynamique, IPSL, Sorbonne Universités, UPMC Univ  
 Paris 06, CNRS, 4 place Jussieu, 75005 Paris, France.*

<sup>c</sup>*Southwest Research Institute, Boulder, CO 80302, United States*

<sup>d</sup>*Lowell Observatory, Flagstaff, AZ, United States*

<sup>e</sup>*Université Grenoble Alpes, CNRS, CNES, Institut de Planétologie et  
 Astrophysique de Grenoble, F-38000 Grenoble, France*

<sup>f</sup>*Department of Physics, University of Idaho 875 Perimeter Drive, Moscow, ID  
 83843, United States*

<sup>g</sup>*Department of Earth, Atmospheric, and Planetary Sciences, Massachusetts  
 Institute of Technology, Cambridge, MA 02139, United States*

<sup>h</sup>*Johns Hopkins University Applied Physics Laboratory, Laurel, MD, 20723,  
 United States*

Copyright © 2005, 2006 Ross A. Beyer, David P. O'Brien, Paul Withers, and Gwen Bart

---

Number of pages: 47  
 Number of tables: 2  
 Number of figures: 18

**Proposed Running Head:**

**Please send Editorial Correspondence to:**

Tanguy Bertrand

National Aeronautics and Space Administration (NASA), Ames Research Center, Space Science Division, Moffett Field, CA 94035, United States

Email: [tanguy.bertrand@nasa.gov](mailto:tanguy.bertrand@nasa.gov)

## ABSTRACT

Pluto’s surface is covered in numerous CH<sub>4</sub> ice deposits, that vary in texture and brightness, as revealed by the New Horizons spacecraft as it flew by Pluto in July 2015. These observations suggest that CH<sub>4</sub> on Pluto has a complex history, involving reservoirs of different composition, thickness and stability controlled by volatile processes occurring on different timescales. In order to interpret these observations, we use a Pluto volatile transport model able to simulate the cycles of N<sub>2</sub> and CH<sub>4</sub> ices over millions of years. By assuming fixed solid mixing ratios, we explore how changes in surface albedos, emissivities and thermal inertias impact volatile transport. This work is therefore a direct and natural continuation of the work by Bertrand et al. (2018), which only explored the N<sub>2</sub> cycles. Results show that bright CH<sub>4</sub> deposits can create cold traps for N<sub>2</sub> ice outside Sputnik Planitia, leading to a strong coupling between the N<sub>2</sub> and CH<sub>4</sub> cycles. Depending on the assumed albedo for CH<sub>4</sub> ice, the model predicts CH<sub>4</sub> ice accumulation (1) at the same equatorial latitudes where the Bladed Terrain Deposits are observed, supporting the idea that these CH<sub>4</sub>-rich deposits are massive and perennial, or (2) at mid-latitudes (25°-70°), forming a thick mantle which is consistent with New Horizons observations. In our simulations, both CH<sub>4</sub> ice reservoirs are not in an equilibrium state and either one can dominate the other over long timescales, depending on the assumptions made for the CH<sub>4</sub> albedo. This suggests that long-term volatile transport exists between the observed reservoirs. The model also reproduces the formation of N<sub>2</sub> deposits at mid-latitudes and in the equatorial depressions surrounding the Bladed Terrain Deposits, as observed by New Horizons. At the poles, only seasonal CH<sub>4</sub> and N<sub>2</sub> deposits are obtained in Pluto’s current orbital configuration. Finally, we show that Pluto’s atmosphere always contained, over the last astronomical cycles, enough gaseous CH<sub>4</sub> to absorb most of the incoming Lyman- $\alpha$  flux.

*Keywords:* Pluto; CH<sub>4</sub>; paleoclimate; Modeling; GCM; glacier; volatile transport ;

<http://icarus.cornell.edu/information/keywords.html>

# 1 Introduction

## 1.1 *Pluto’s ices as observed by New Horizons in 2015*

In July 2015, our vision of Pluto changed as the New Horizons spacecraft revealed a frozen world with unprecedented landscapes in the Solar System (Stern et al., 2015). The first analysis of spectral data from the Linear Etalon Imaging Spectral Array (LEISA) instrument on-board New Horizons showed that Pluto’s water ice bedrock is covered by volatile ices such as  $\text{N}_2$ ,  $\text{CH}_4$  and  $\text{CO}$ , except in some parts of the equatorial regions, covered only by dark tholins (Grundy et al., 2016). Detailed spectroscopic analysis then revealed a more complex volatile ice distribution with different types of ice mixtures on Pluto’s surface (Schmitt et al., 2017; Protopapa et al., 2017).

The exact nature of the observed deposits is not easy to derive from these spectroscopic analyses, because they involve many parameters such as the abundance, dilution state, texture, or grain size, which are poorly constrained (Schmitt et al., 2017). A first extraction of these parameters at the global scale is solved through sophisticated inversion of a Hapke’s radiative transfer model of the LEISA data (Protopapa et al., 2017). However, spectroscopic analyses of the surface do not provide information about the thickness of these deposits. The thickness can be inferred from geological insights using high resolution images from the LOng-Range Reconnaissance Imager (LORRI) instrument and albedo maps, that help distinguish a thin frost of ice from a massive deposit. A simplified global picture of the volatile ice reservoirs on Pluto is shown in Figure 1.

The most prominent volatile ice deposit on Pluto’s surface is a kilometer-thick ice sheet made of  $\text{N}_2$  ice, mixed with  $\text{CH}_4$  and  $\text{CO}$ , which is sequestered in Sputnik Planitia<sup>1</sup>, the vast topographic basin at the anti-Charon longitude (Stern et al., 2015; Grundy et al., 2016). This perennial glacier is the main reservoir of  $\text{N}_2$  ice.

Methane is detected almost everywhere in the northern hemisphere, with varying brightness, textures and mixtures (such as  $\text{CH}_4$ -rich ice and  $\text{CH}_4$  diluted in  $\text{N}_2$ -rich ice), as highlighted in the available maps of the equivalent width of absorption in the Multi-spectral Visible Imaging Camera (MVIC)  $\text{CH}_4$  filter (Grundy et al., 2016; Earle et al., 2018b) as well as in LEISA maps (Protopapa et al., 2017; Schmitt et al., 2017).

The North Pole is covered by relatively pure and bright  $\text{CH}_4$ -rich ice, with an

---

<sup>1</sup> The place names mentioned in this paper include a mix of officially approved names and informal names.

estimated Bond albedo higher than 0.7 (Buratti et al., 2017).

The mid-latitudes plains (25°N-70°N) are covered in mixtures of N<sub>2</sub>-rich and CH<sub>4</sub>-rich ices following a latitudinal trend (Schmitt et al., 2017; Protopapa et al., 2017; Earle et al., 2018b). The latitudes 55°N-70°N are enriched in CH<sub>4</sub>, with few N<sub>2</sub>-rich deposits mostly confined in the depressions. The latitudes 35°N-55°N are dominated by N<sub>2</sub>-rich ices, while the latitudes 25°N-35°N are covered again mainly of CH<sub>4</sub>-rich ices Protopapa et al. (2017). Interestingly, the CH<sub>4</sub>-rich deposits in these regions seem to form a relatively thick mantle, maybe 100-1000 m, given the fact that they cover some craters and give to the surface a smooth aspect.

The equatorial regions (25°S-25°N) show a greater diversity of terrains in longitude, in terms of albedo (Buratti et al., 2017), color (Olkin et al., 2017) and composition (Schmitt et al., 2017). Outside Sputnik Planitia, in the region of Tartarus Dorsa (East of Tombaugh Regio, 5°S-28°N), relatively pure CH<sub>4</sub>-rich ice has been detected in the Bladed Terrain Deposits (BTD, Moore et al., 2018; Schmitt et al., 2017; Protopapa et al., 2017; Earle et al., 2018b). These terrains are characterized by parallel sets of steep ridges and sharp crests and are situated on high ground (above 2 km), which may indicate very massive CH<sub>4</sub>-rich deposits, at least 300 m thick (Moore et al., 2018). They are relatively dark, with an estimated Bond albedo between 0.5-0.6 (Buratti et al., 2017). Their distinctive texture on Pluto’s maps suggests that they extend further east, from longitudes 210°E to 40°E, and further south, down to 25°S (see Fig. 3 in Olkin et al., 2017; Moore et al., 2018). They also seem to be interspersed with N<sub>2</sub>-rich flat-floored bright plains located in the depressions and valleys of these regions.

Finally, the eastern part of Tombaugh Regio (between Sputnik Planitia and Tartarus Dorsa) is bright and also contains N<sub>2</sub>-rich and CH<sub>4</sub>-rich ices with N<sub>2</sub> mostly detected in the depressions (Schmitt et al., 2017; Protopapa et al., 2017).

These observations raise the following questions: What drives the observed ice distribution and the diversity of N<sub>2</sub>-rich and CH<sub>4</sub>-rich terrains? Are these reservoirs perennial (lasting for many Pluto years, e.g. glaciers) or seasonal (disappearing over one Pluto year, e.g. frosts)? How do they evolve over astronomical and seasonal timescales? In this paper, we aim to provide answers to these questions by simulating the long-term evolution of N<sub>2</sub> and CH<sub>4</sub> ice, using the Pluto volatile transport model developed at the Laboratoire de Météorologie Dynamique (LMD, Bertrand and Forget, 2016; Bertrand et al., 2018).

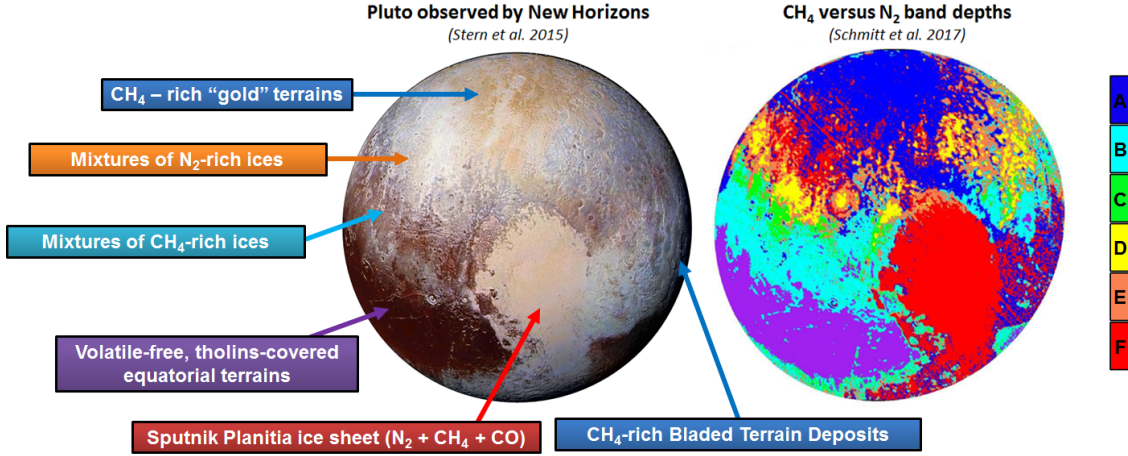


Fig. 1. The different types of terrains observed on Pluto (left) and the associated N<sub>2</sub>-CH<sub>4</sub> mixtures (right). The color scale is described in details in (Schmitt et al., 2017): **A-B** relatively pure CH<sub>4</sub> ice, or N<sub>2</sub>-rich ice with grains < few cm and CH<sub>4</sub> > 1%. **D-E** large N<sub>2</sub>-rich grains (> 10 cm) with small amount of CH<sub>4</sub> (0.1-1%). **C** N<sub>2</sub>-rich ice with both medium N<sub>2</sub> grain size (< few cm) and CH<sub>4</sub> < 1%. **F** very large N<sub>2</sub> ice grains (> 20 cm) with CH<sub>4</sub> > 1%.

## 1.2 Modeling of volatile transport on Pluto

Global volatile transport models of Pluto have been used to explain how changes in insolation over the course of Pluto’s orbit affect the surface and subsurface temperatures (which plays a key role in the Pluto environment), resulting in latitudinal variations of distribution of volatile ices (Young, 1993; Hansen and Paige, 1996; Spencer et al., 1997; Young, 2012, 2013; Hansen et al., 2015; Toigo et al., 2015; Olkin et al., 2015; Bertrand and Forget, 2016; Bertrand et al., 2018).

In particular, Bertrand and Forget (2016) (hereinafter referred as BF2016) simulated the transport of N<sub>2</sub>, CH<sub>4</sub> and CO ices over tens of thousands Earth years and obtained a seasonal cycle that reproduces, to first order, the ices distribution observed by New Horizons in 2015. They showed that N<sub>2</sub> ice inevitably accumulates inside Sputnik Planitia basin, because of an atmosphere-topography process: the N<sub>2</sub> surface pressure and condensing temperature are higher at the bottom of the basin than outside, and therefore the N<sub>2</sub> deposits in the basin are warmer and loose more energy by thermal infrared cooling, which is balanced by a stronger N<sub>2</sub> condensation at that location (so that enough latent heat is released to ensure that the surface remains at the equilibrium temperature). In their simulations, the equatorial regions (apart from Sputnik Planitia) always remained warmer than at least one of the two poles (at any given time) and therefore no volatile condensed there, which explained

the dark equatorial band of Pluto. They also showed that the lower volatility of  $\text{CH}_4$  ice at Pluto’s surface temperatures allows it to exist elsewhere than in the Sputnik Planitia ice sheet, forming frost even at locations where  $\text{N}_2$  ice would immediately sublime. In their model,  $\text{CH}_4$  ice seasonally covered both hemispheres, and, if its albedo was high enough,  $\text{N}_2$  was able to condense on it and form a latitudinal band around  $45^\circ\text{N}$  in 2015, in agreement with New Horizons observations (Figure 1). This impact of the ice albedo is also highlighted by Earle et al. (2018a), who suggest that runaway albedo variations are more efficient in the equatorial regions than at the poles, forming stark contrasts in albedo and volatile abundance.

However, the simulations performed in BF2016, and in most previous volatile transport modeling studies on Pluto, had two main limitations. First, they only considered small amounts of ice and were therefore not able to reproduce the formation of perennial glaciers. For instance, the globally averaged volatile ice reservoir used in BF2016 is only of few millimeters, in order to reach a steady state over the annual timescale. Secondly, they only focused on the  $10^4$  Earth years timescales, with the present orbital and obliquity parameters. Yet Pluto’s high obliquity (currently around  $119.6^\circ$ ) varies by about  $23^\circ$  over a period of 2.8 millions of Earth years (2.8 Myrs herein refers to the astronomical timescale) while Pluto’s longitude of perihelion regresses by  $360^\circ$  over 3.7 Myrs (Dobrovolskis et al., 1997; Spencer et al., 1997). Both parameters impact the duration and intensity of the seasons, and the latitudes where volatile ices accumulate (Binzel et al., 2017; Earle et al., 2017).

Recently, Bertrand et al. (2018) (hereinafter referred as B2018) improved the Pluto volatile transport model described in BF2016 by implementing the most recent topography data of Pluto, the variations of obliquity, longitude of perihelion and eccentricity with time, and by taking into account a realistic  $\text{N}_2$  reservoir as well as a  $\text{N}_2$  ice viscous flow model. Thanks to this modeling effort, they explored the cycles of  $\text{N}_2$  over several astronomical cycles (up to 30 Myrs). Their results explained many geological features of Sputnik Planitia, such as the evidence of recent and past glacial flow and erosion, the presence of sublimation pits in the southern portion of the ice sheet, as well as the brightness and composition of the surface ice. They also showed that large  $\text{N}_2$  ice deposits can remain relatively stable and persist over tens of millions of years in the equatorial regions or over mid-latitudinal bands, in particular at low elevations.

### 1.3 Objectives of this paper

In this paper, we want to carry this work forward and explore the  $\text{CH}_4$  cycles over astronomical and seasonal timescales with the latest version of the Pluto

volatile transport model. In particular, our objectives are:

- (1) To determine the latitudes where  $\text{CH}_4$  ice tends to accumulate over millions of years.
- (2) To investigate how the  $\text{CH}_4$  albedo impacts the  $\text{N}_2$  condensation-sublimation cycles and the latitudinal ices distribution.
- (3) To compare our results with New Horizons observations of Pluto’s surface (e.g. [Stern et al., 2015](#); [Grundy et al., 2016](#); [Moore et al., 2016](#)), explain the observed latitudinal distribution of volatile ices ([Schmitt et al., 2017](#); [Protopapa et al., 2017](#)), infer the nature (perennial or seasonal) of the observed deposits, and discuss the possible scenarios for their formation.

To fulfill these objectives, we adapt the Pluto volatile transport model described in B2018 so that it also takes into account the  $\text{CH}_4$  cycle. In Section 2, we detail the recent model improvements, the assumptions made and the simulation settings. The results are presented in two independent sections. We first perform simulations with a global uniform  $\text{CH}_4$  ice albedo (Section 3). Then, we perform simulations with two  $\text{CH}_4$  albedo values (Section 4) depending on the latitude of the deposit, with a low value in the equatorial regions (old dark deposits) and high values in the mid-to-polar regions (bright deposits, above  $30^\circ$ ). Our results are summarized in Table 2, and discussed in Section 5.

## 2 The Pluto volatile transport model

We use the latest version of the LMD Pluto volatile transport model, as described in BF2016, B2018 and [Forget et al. \(2017\)](#). The model settings are similar to those in B2018 except for the following changes, summarized in Table 1.

### 2.1 General settings of the simulations

The simulations of this paper are performed on a horizontal grid of  $32 \times 24$  points, which corresponds to a grid-point spacing of  $7.5^\circ$  in latitude by  $11.25^\circ$  in longitude (about 150 km at the equator). We perform simulations over 30 Myrs using the paleoclimate mode, the  $\text{N}_2$  ice viscous flow scheme and the ice equilibration algorithm described in details in B2018: the model is run over 5 Pluto years, then the annual mean ice rate of the last Pluto year is used to estimate the new amounts of ice over a paleo-timestep  $\Delta t$  and finally the topography is updated according to the new amounts of ice and the orbital parameters and the obliquity of Pluto are changed according to the new epoch  $t + \Delta t$ . The maximal change of obliquity within  $\Delta t$  must remain lower than



the latitudinal resolution used. Here we use  $\Delta t = 100,000$  Earth years, that is about 400 Pluto orbits, allowing fast computing times and reasonable time resolution, with a maximal change of obliquity within that timeframe of about  $3^\circ$  (Binzel et al., 2017).

Most of the atmospheric effects are neglected in the model (clouds, radiative effect of the atmosphere...). As in BF2016, volatile transport occurs through the atmosphere via a parametrization of the atmospheric circulation, using a characteristic timescale  $\tau_{CH_4} = 10^7$  s (about four terrestrial months) to globally mix gaseous  $CH_4$ .

<b>Paleo-timestep</b>	$\Delta t = 100,000$ Earth years
<b>Reservoirs</b> (global average)	$R_{N_2} = 300$ m <sup>a</sup> $R_{CH_4} = 4$ m <sup>b</sup>
<b>Albedo</b>	$A_{N_2} = 0.7$ $A_{CH_4} = 0.5-0.8$ $A_{bedrock} = 0.1$
<b>Emissivity</b>	$\epsilon_{N_2} = 0.8$ $\epsilon_{CH_4} = 0.8$ $\epsilon_{bedrock} = 1$
<b>Thermal inertia</b>	TI=400-1500 SI <sup>c</sup>
<b>Atmospheric mixing timescale</b>	$\tau_{N_2} = 1$ s $\tau_{CH_4} = 10^7$ s
<b>CH<sub>4</sub> ice mixing ratio in N<sub>2</sub></b>	0.5 %

---

<sup>a</sup> Fills Sputnik Planitia up to 2500 m below the mean surface level  
<sup>b</sup> In Section 4, an infinite reservoir is used  
<sup>c</sup>  $SI = J s^{-0.5} m^{-2} K^{-1}$

Table 1

Settings and surface conditions assumed in our simulations. In this work we assess the impact of subsurface thermal inertia and  $CH_4$  ice albedo.

## 2.2 Assumptions on the state of $N_2$ and $CH_4$ ice in the model

On Pluto,  $CH_4$  and  $N_2$  easily mix together and are not expected to exist in perfectly pure state (Trafton, 2015; Tan and Kargel, 2018). Analysis of the New Horizons LEISA spectral observations of Pluto’s surface has been performed using sophisticated spectral models and reveal complex mixtures in different amounts, also involving CO and contamination by tholins (Grundy et al., 2016; Protopapa et al., 2017; Schmitt et al., 2017). Most of the volatile ice covering Pluto’s surface seems to be dominated by  $N_2$ -rich: $CH_4$  (e.g. Sputnik Planitia) or  $CH_4$ -rich: $N_2$  (e.g. the north pole). Observations also suggest mixtures of both  $N_2$ -rich +  $CH_4$ -rich at some locations, but the exact nature of these deposits is uncertain for now because they could fall into three distinct possible categories: (1) intimate mixture or intermolecular mutual attraction, at the grain scale, (2) geographic mixtures ( $N_2$ -rich +  $CH_4$ -rich could be observed at the pixel scale but not be mixed, strictly speaking, as they could be spatially disconnected at smaller scales), (3) stratification (a thin layer of  $CH_4$ -rich ice could form at the top of a  $N_2$ -rich deposit).

The scenario of intimate mixtures suggests a perfect thermodynamic equilibrium of two types of crystals at significant depth, strictly following the binary phase diagram. This is typical of instantaneous thermodynamic equilibrium but should not apply to Pluto, which we believe is a non-equilibrium dynamical environment with continuous exchange of materials. Instead,  $\text{CH}_4$ -rich and  $\text{N}_2$ -rich ices may co-exist because of dynamical processes such as sublimation, which would lead to stratification ( $\text{N}_2$  sublimation leaving  $\text{CH}_4$  behind and leading to a  $\text{CH}_4$ -rich ice layer on top of the  $\text{N}_2$ -rich ice).

However, the mechanisms controlling the formation and evolution of such  $\text{N}_2$ -rich +  $\text{CH}_4$ -rich mixtures remain largely unknown. With regards to this, the model presented in this paper is rather simple. As in BF2016, it does not compute any evolution of ice mixing ratio. In the simulations, the surface is either volatile-free, covered by pure  $\text{CH}_4$  ice or by  $\text{N}_2$ -rich: $\text{CH}_4$  ice. Pure  $\text{CH}_4$  ice is an approximation for unsaturated  $\text{CH}_4$ -rich ice. We make the approximation that such a  $\text{CH}_4$ -rich ice behaves almost like pure  $\text{CH}_4$  ice, in terms of temperature and vapor pressure at saturation of  $\text{CH}_4$ . It can form after sublimation of  $\text{N}_2$  ice (in which it was trapped before) or directly on a volatile-free surface (its lower volatility than  $\text{N}_2$  allows it to condense where  $\text{N}_2$  would instantly sublime). For instance,  $\text{CH}_4$ -rich ice has been observed on top of mountains in the region of Chtulhu, where  $\text{N}_2$  could not have condensed at first (because of the significantly high altitude and low albedo of these terrains).

When both  $\text{CH}_4$  and  $\text{N}_2$  ices are present on the surface, we assume that  $\text{CH}_4$  is diluted in a solid solution  $\text{N}_2$ : $\text{CH}_4$  with 0.5% of  $\text{CH}_4$ , as retrieved from telescopic observations (Merlin, 2015) and overall from the New horizons LEISA spectroscopic data (see spectra g and j in Table 3 in Protopapa et al., 2017). This modeled  $\text{N}_2$ -rich: $\text{CH}_4$  ice sublimates by conserving the 0.5% of diluted  $\text{CH}_4$ . In the next sections of this paper, we refer to this phase as  $\text{N}_2$  ice.

The impact of  $\text{N}_2$ -rich +  $\text{CH}_4$ -rich mixtures is out of the scope of this paper, and we neglect their effect in the model. By doing so, we assume that this state corresponds to a short transient phase. In the future, we plan to investigate further stratification mechanisms and implement them in the volatile transport model. To do this, experimental studies of these processes are also strongly needed.

### 2.3 Surface properties

As in B2018, we use a reference  $\text{N}_2$  ice albedo and emissivity which remain fixed to 0.7 and 0.8 respectively. The surface  $\text{N}_2$  pressure simulated in the model is constrained by these values. The albedo and emissivity of the bare ground (volatile-free surface) are set to 0.1 and 1 respectively, which corresponds to

a terrain covered by dark tholins such as Cthulhu. CH<sub>4</sub> ice emissivity is fixed to 0.8 in all simulations, but we explore different values of CH<sub>4</sub> ice albedo, ranging from 0.3 to 0.8 depending on the simulation (the reference albedo is 0.5). Note that CO is also transported by the model, but plays no role, as we assume it always “follows” N<sub>2</sub>.

The reference seasonal thermal inertia (TI) of the subsurface is uniformly set to 800 SI, as in B2018. However we also performed simulations using a uniform soil TI set to 400 or 1200 SI (Section 3.3), and simulations in which each type of terrain (water ice bedrock, N<sub>2</sub> or CH<sub>4</sub> ice) has its own TI ranging from 400 to 1200 SI (see Table 2 and Section 4.6).

We also tested some scenarios in which the N<sub>2</sub> ice surface emissivity depends on its temperature and crystalline phase (e.g. simulation #TI888\_050\_065\_phase). We assumed a minimal emissivity of  $\varepsilon_\alpha=0.3$  when the ice is in its  $\alpha$ -phase, with a surface temperature  $T_s$  below the transition temperature of  $T_{\alpha-\beta}=35.6$  K and a maximal emissivity of  $\varepsilon_\beta=0.8$  in its  $\beta$ -phase, based on the results from [Stansberry and Yelle \(1999\)](#). We use a simple hyperbolic tangent function for the transition:

$$\varepsilon_{N_2} = \frac{1}{2} [1 + \tanh(3(T_{\alpha-\beta} - T_s))] (\varepsilon_\alpha - \varepsilon_\beta) + \varepsilon_\alpha \quad (1)$$

As predicted by [Stansberry and Yelle \(1999\)](#), the N<sub>2</sub> ice surface temperature in these simulations remains at the transition temperature of 35.6 K during most of Pluto’s northern fall and winter, because the emissivity change leads to a negative feedback of surface temperatures. The exchange of latent heat between both phases also leads to a negative feedback and plays a role in locking the temperature to the transition, but here we neglect this effect for sake of simplicity. Note that the  $\alpha$ -phase of N<sub>2</sub> ice has never been observed in the outer solar system. Here we only test the case of an extremely low emissivity for N<sub>2</sub> ice in  $\alpha$ -phase, which enables us to assess the maximum possible effect of this change on Pluto’s climate.

## 2.4 Reservoirs

All simulations are run with N<sub>2</sub> ice initially placed in Sputnik Planitia in a  $\sim 10$  km deep elliptical basin, as described in B2018. N<sub>2</sub> ice fills this modeled basin up to 2.5 km below the mean surface level, which corresponds to a global N<sub>2</sub> reservoir of  $\sim 300$  m. N<sub>2</sub> is allowed to condense and sublime everywhere on Pluto’s surface, depending on the computed local surface thermal balance.

The simulations performed with a uniform CH<sub>4</sub> ice albedo (Section 3) use a global CH<sub>4</sub> reservoir of  $2000 \text{ kg m}^{-2}$ , which corresponds to 4 m, if we assume

a  $\text{CH}_4$  ice density of  $500 \text{ kg m}^{-3}$  (Leyrat et al., 2016). This amount is low compared to the total reservoir of  $\text{CH}_4$  ice expected on Pluto. Indeed, the BTM only could correspond to a reservoir of 22 m on global average if we assume that they cover an equatorial surface equivalent to  $10^\circ$  in latitudes and  $180^\circ$  in longitudes and that they are only 500 m thick. This is a lower limit for  $\text{CH}_4$  ice, since the BTM may be thicker and since other km-thick reservoirs may exist in the mid-latitudinal regions. However, running simulations with such a  $\text{CH}_4$  ice reservoir is challenging, because the  $\text{CH}_4$  condensation-sublimation rates are very low. Typically, one meter of  $\text{CH}_4$  ice evolves over one million years. Therefore the total amount of  $\text{CH}_4$  ice in our simulations is a trade-off between having the largest possible reservoir and reaching a steady state for ice distribution within tens of Myrs.

Alternatively, the simulations performed with a dual  $\text{CH}_4$  ice albedo (Section 4) are initialized with an infinite source of  $\text{CH}_4$  ice at the location of the observed BTM in the equatorial regions.

## 2.5 Other settings related to the $\text{CH}_4$ cycle

The model does not allow  $\text{CH}_4$  ice to flow and the topography does not change according to the accumulation or loss of  $\text{CH}_4$  ice (it only changes according to the variation of  $\text{N}_2$  ice thickness). These choices are driven by the fact that (1) the  $\text{CH}_4$  reservoir involved in the model is relatively low (see above) and (2) the  $\text{CH}_4$  ice may be too rigid to lead to a significant glacial flow activity (Eluszkiewicz and Stevenson, 1990; Moore et al., 2017, 2018), as suggested by the steep slopes of the BTM’s ridges ( $20^\circ$ ), which is also why these terrains are described as massive deposits instead of glaciers.

Finally, for the simulations performed with a uniform  $\text{CH}_4$  ice albedo (Section 3), we prohibit  $\text{CH}_4$  to condense in the Sputnik Planitia  $\text{N}_2$  ice sheet (we do not allow any  $\text{CH}_4$  in SP). By doing this, we prevent the entire  $\text{CH}_4$  reservoir to be trapped in Sputnik Planitia after several Myrs and we always conserve the same mass of  $\text{CH}_4$  ice outside the basin. On Pluto, mechanisms or other sources must exist to maintain a certain amount of  $\text{CH}_4$  ice outside Sputnik Planitia (see Discussions in Section 5). For instance, saturation of  $\text{N}_2$ -rich ice with  $\text{CH}_4$ , or formation of a  $\text{CH}_4$ -rich layer on top of  $\text{N}_2$ -rich ice are processes that could limit further condensation of  $\text{CH}_4$  in SP, and maintain significant amounts of  $\text{CH}_4$  ice outside SP.

### 3 Simulations with a uniform CH<sub>4</sub> ice albedo

In this section we investigate where CH<sub>4</sub> ice tends to accumulate over astronomical timescales.

#### 3.1 Initial state of the simulation

The simulations are performed using the New Horizons topography data, starting with all N<sub>2</sub> ice filling a deep modeled Sputnik Planitia basin up to 2.5 km below the mean surface level, and with a 4-meter thick layer of CH<sub>4</sub> ice covering the entire globe. The simulation is performed with a unique albedo for CH<sub>4</sub> ice, set to 0.5, and a uniform thermal inertia of 800 SI. We then let the volatile ices evolve over 30 Myrs.

#### 3.2 Results: formation of massive equatorial deposits and mid-to-polar frosts of CH<sub>4</sub>

Figure 2 shows the evolution of the CH<sub>4</sub> ice distribution obtained over the last 30 Myrs. The ice quickly accumulates in the equatorial regions. Typically, after 10 Myrs, 20-40 m thick CH<sub>4</sub> deposits ( $1\text{-}2 \times 10^4 \text{ kg m}^{-2}$ ) are formed between 12°S-22.5°N (by accumulation of the CH<sub>4</sub> ice which was initially placed at the poles). The maximal net rates of sublimation are obtained at the poles. Above 30° latitude, 4 meters of ice can disappear within one astronomical cycle (2.8 Myrs). By extrapolation, if we had started with a global CH<sub>4</sub> ice reservoir of 100 m, we would have obtained  $\sim 1$  km thick deposits in the equatorial regions after 50-100 Myrs.

Why is CH<sub>4</sub> ice accumulating at the equator? Because of Pluto’s high obliquity, ranging from 104° to 127° over 2.8 Myrs, the polar regions receive more solar flux than the equator on average. If one assumes medium to large soil thermal inertia, this leads to colder equatorial regions on average over several Myrs (see Fig. 4.B in B2018). In addition to the obliquity cycle, Pluto’s solar longitude of perihelion ( $L_{speri}$ ) oscillates over a period of 3.7 Myrs and leads to asymmetries in the seasons (Dobrovolskis et al., 1997; Binzel et al., 2017). For instance, when Pluto’s  $L_{speri}$  is close to 90°, the northern polar latitudes undergoes a short and intense summer (close to the perihelion) and a long and intense winter (close to the aphelion) while the southern polar latitudes undergoes a long summer far from the sun and a short winter close to the sun, and vice versa when the orbital conditions are reversed ( $L_{speri}$  close to 270°). As a result, the northern hemisphere tends to be colder on annual average when

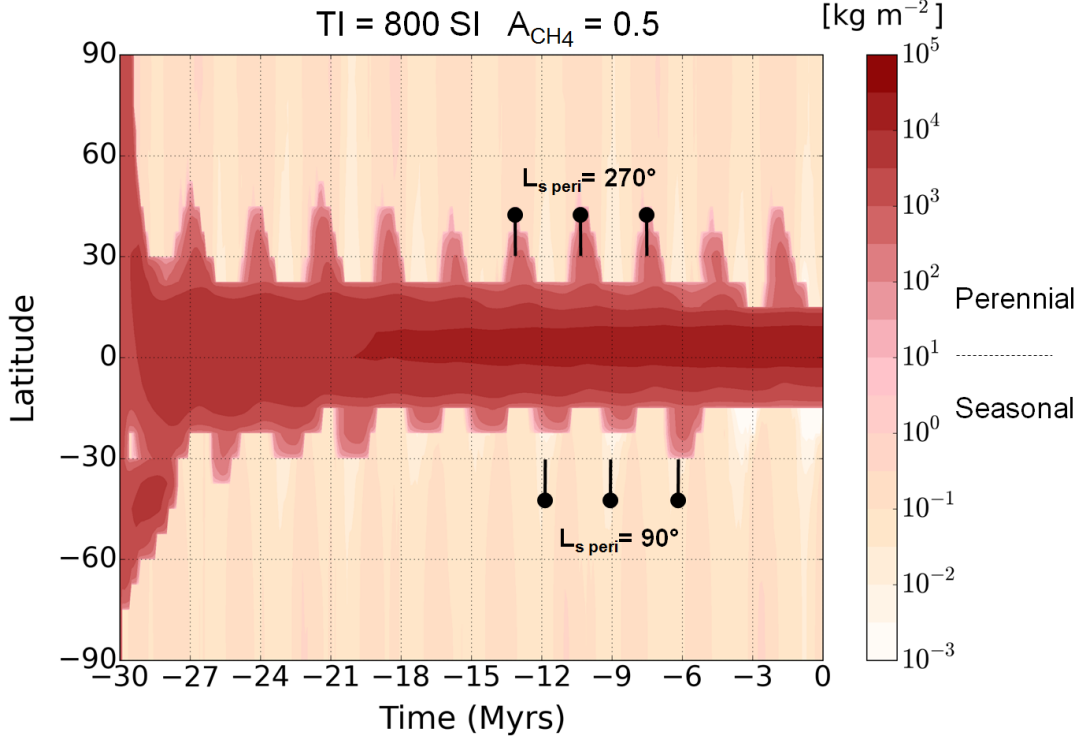


Fig. 2. Evolution over 30 Myrs of the perennial and seasonal deposits of  $\text{CH}_4$  ice on Pluto in our simulation with a unique  $\text{CH}_4$  ice albedo of 0.5 (the values shown correspond to the zonal annual mean amount of  $\text{CH}_4$  ice in  $\text{kg m}^{-2}$ , for the areas outside of Sputnik Planitia).  $\text{CH}_4$  ice quickly accumulates in the equatorial regions, where it forms massive deposits. At higher latitudes, only thin seasonal  $\text{CH}_4$  deposits form. The black vertical lines indicate the periods where  $L_{\text{speri}}$  is close to  $90^\circ$  and  $270^\circ$  (when seasonal asymmetries are the strongest).

Pluto's  $L_{\text{speri}}$  is close to  $90^\circ$ , and warmer when Pluto's  $L_{\text{speri}}$  is close to  $270^\circ$  (see Fig. 4.A in B2018).

However, our results show that when  $L_{\text{speri}}$  is close to  $90^\circ$ , the intense northern summer (occurring close to the perihelion) removes a significant amount of  $\text{CH}_4$  ice at the north pole and during this epoch  $\text{CH}_4$  ice accumulates at the equator and in the southern hemisphere. Conversely, when  $L_{\text{speri}}$  is close to  $270^\circ$ ,  $\text{CH}_4$  accumulates at the equator and in the northern hemisphere. This is illustrated by Figure 2 showing that  $\text{CH}_4$  deposits extend to higher latitudes ( $20^\circ\text{S}$  and  $45^\circ\text{N}$ ) during the periods of asymmetric seasons ( $L_{\text{speri}}$  close to  $90^\circ$  or  $270^\circ$ ).

On average over one astronomical cycle, the equatorial regions are a net accumulation zone of  $\text{CH}_4$  ice, while the poles are a net sublimation zone. This result is consistent with New Horizons observations of the  $\text{CH}_4$ -rich BTB in the equatorial regions (Moore et al., 2016, 2018) and supports the fact that they are thick and perennial  $\text{CH}_4$  deposits.

Figure 2 also shows that the modeled  $\text{CH}_4$  deposits are not symmetric to the equator, as they tend to be more extended to the northern latitudes, in accordance with the observed latitudinal extent of the BTD ( $5^\circ\text{S}$ - $25^\circ\text{N}$ ). This is because during the last 70 Myrs, the  $L_{\text{peri}}$  value at high obliquity remained close to  $90^\circ$  and led to an asymmetry of insolation and surface temperatures which favors a slightly warmer south hemisphere (see details and Fig. 5 in B2018, and Discussions in Section 5).

Note that our modeling does not reproduce the bladed aspect of the BTD nor explain why they are mostly located in the eastern hemisphere, although it may be due to the fact that the dark tholin-covered surface in the western hemisphere (Cthulhu) prevents condensation of  $\text{CH}_4$  (assuming that the BTD formed after Cthulhu). It is likely that this longitudinal asymmetry has dynamical origins and therefore it should be investigated by using 3D global climate models (which include a full 3D dynamical core).

Although thick deposits of  $\text{CH}_4$  ice are not stable at the poles, thin  $\text{CH}_4$  frost ( $< 1$  mm) always form there seasonally, as illustrated by Figure 2. They form during fall-winter, when the equatorial deposits and the  $\text{CH}_4$  frosts at the opposite pole (spring-summer) feed the atmosphere with gaseous  $\text{CH}_4$ . In BF2016, a similar result was obtained but because the simulations were not performed with a large enough reservoir of  $\text{CH}_4$  ice, no thick deposit was obtained at the equator and the polar frosts disappeared in the early spring.

### 3.3 Sensitivity to the reservoir, soil thermal inertia and $\text{CH}_4$ ice albedo

Changing the initial spatial distribution of  $\text{CH}_4$  ice (e.g. only at the poles, or over a specific longitudinal or latitudinal band) does not impact the results:  $\text{CH}_4$  ice would still accumulate at the equator, with a slight extent to northern latitudes, while mm-thin deposits would form elsewhere during polar winter. If we increase the  $\text{CH}_4$  reservoir, then thicker  $\text{CH}_4$  deposits are obtained at the equator. The  $\text{CH}_4$  mid-to-polar frosts remain qualitatively and quantitatively the same year after year because they are controlled by the location of the equatorial deposits.

Changing the albedo of  $\text{CH}_4$  ice leads to major changes in the results. If we lower the uniform  $\text{CH}_4$  ice albedo, the ice becomes warmer, resulting in higher sublimation rates and larger amounts of  $\text{CH}_4$  to be transported to other sinks. In this case, we obtain more extended equatorial deposits and episodic thicker perennial deposits at the poles (see middle panel on Figure 3). If we increase the uniform  $\text{CH}_4$  ice albedo, then  $\text{CH}_4$  ice may become cold enough to trigger  $\text{N}_2$  condensation on it, which strongly impacts both volatile cycles. This effect is explored in Section 4.

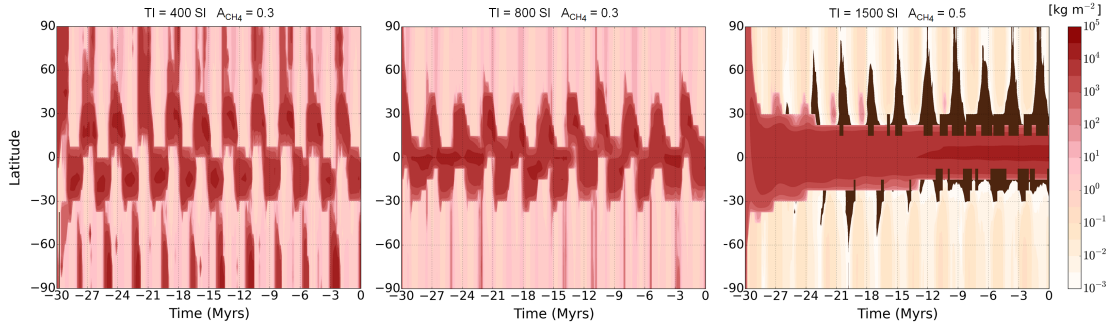


Fig. 3. Same as Figure 2 but assuming a thermal inertia  $TI=400$  SI coupled with a  $CH_4$  ice albedo  $A_{CH_4}=0.3$  (left),  $TI=800$  SI and  $A_{CH_4}=0.3$  (middle),  $TI=1500$  SI and  $A_{CH_4}=0.5$  (right). The low TI case was performed with a lower albedo for  $CH_4$  ice (0.3) in order to limit the effect of  $N_2$  condensation on  $CH_4$  ice (this effect is explored in Section 4). The brown color represents the dark, tholin-covered bedrock.

Results are also sensitive to the soil thermal inertia, as shown in Figure 3. When a high thermal inertia is used ( $> 1500$  SI), surface temperatures tend to be much warmer at the poles than at the equator on average over several Myrs (see B2018) and thus  $CH_4$  ice accumulates closer to the equator, while less frost forms at the poles. When a low thermal inertia is used ( $< 400$  SI), the surface temperatures reach higher values in summer and lower values in winter and tend to be warmer at the equator than at the poles on average over several Myrs. In this case, large perennial reservoirs can form periodically in the mid-to-polar regions. However this case predicts, for present time, large reservoirs of  $CH_4$  ice in the south hemisphere only, which is not consistent with the observations.

#### 4 Simulations with darker $CH_4$ ice near the equator than at mid and high latitudes

$CH_4$  ice is known to play a complex role on Pluto’s climate and volatile ices cycles since it can cold trap  $N_2$  ice if its albedo is high enough (Bertrand and Forget, 2016; Earle et al., 2018a). In our model, the albedo of  $CH_4$  ice is a key sensitivity parameter and we usually represent it by one value only, constant with time. However, on Pluto, the real value is not very well known and varies with time and space, because of different processes involving metamorphism effects, haze-particle settling/contamination (which serves as a darkening agent) and slight differences of composition (Buratti et al., 2017; Stern et al., 2015). As an example,  $CH_4$ -rich ice is much brighter in the mid-to-polar than in the BTD (Buratti et al., 2017).

In this section, we intend to explore this sensitivity and better represent the



cycle of  $\text{CH}_4$  by considering two different albedos for  $\text{CH}_4$  ice in the model, based on a criterion in latitude. In accordance with New Horizons observations, we assume that the mid-to-polar deposits are bright (albedo=0.65-0.8) and that the equatorial massive  $\text{CH}_4$  ice deposits are dark (albedo=0.5-0.65). We also explore the impact of TI on the results (TI=400-1200 SI). The albedos of the volatile-free surface and of  $\text{N}_2$  ice remain always fixed to 0.1 and 0.7 respectively.

The results of this section are summarized in Section 4.7 by Figure 15 and Table 2. Note that all results shown for the current Pluto year are the outcome of 30 Myrs simulations.

#### *4.1 Initial state of the simulations*

$\text{N}_2$  ice is placed in Sputnik Planitia only. We place an unlimited  $\text{CH}_4$  ice reservoir in the equatorial regions roughly at the locations of the observed BTD: 15°S-15°N, 140°W-15°E. The rest of the surface is initially volatile-free (assumed to be a tholin-covered water ice bedrock with an albedo of 0.1). We then run the simulations and let the volatile ices evolve over 30 Myrs.

#### *4.2 Reference simulation: accumulation of $\text{CH}_4$ ice at mid-latitudes*

Our reference simulation is named #TI888\_050\_072, which means that is the simulation performed with a thermal inertia (TI) of 800 SI for  $\text{N}_2$ ,  $\text{CH}_4$  and water ices, an albedo for  $\text{CH}_4$  equatorial deposits of 0.5 and an albedo for  $\text{CH}_4$  mid-to-polar deposits of 0.72.

##### *4.2.1 The astronomical cycles of $\text{CH}_4$*

Figure 4 shows the evolution of the perennial  $\text{CH}_4$  (in red) and  $\text{N}_2$  (blue markers) ice deposits obtained over the last 12 Myrs. In this reference simulation, mid-to-polar  $\text{CH}_4$  deposits form at higher latitudes than 30°. Below, the equatorial regions remain volatile-free or covered by the modeled BTD, which is consistent with the observation of dark equatorial regions on Pluto (e.g Cthulhu). These  $\text{CH}_4$  deposits are cold enough to trigger  $\text{N}_2$  condensation and allow the formation of perennial or seasonal  $\text{N}_2$  deposits. Those located around 30°N or 30°S remain perennial at all times, while those located at higher latitudes remain perennial only during 1-2 Myrs during each astronomical cycle, as shown in Figure 4. Note that these perennial  $\text{N}_2$  ice deposits remain less than 15 m thick, as shown in Table 2. At the North Pole, thin perennial  $\text{CH}_4$

deposits ( $< 1$  m) alternate with seasonal deposits over an astronomical cycle. Between  $60^\circ\text{N}$ - $75^\circ\text{N}$ , perennial  $\text{CH}_4$  ice deposits ( $< 1$  m) remain stable with time, while at northern mid-latitudes ( $25^\circ\text{N}$ - $60^\circ\text{N}$ ), a net accumulation of  $\text{CH}_4$  ice is obtained (Figure 4.B). The stability and accumulation of  $\text{CH}_4$  ice at these latitudes is due to (1) the condensation of  $\text{N}_2$  ice on top of the bright  $\text{CH}_4$  ice, which is able to protect  $\text{CH}_4$  from sublimation during most of the year and cold-trap even more  $\text{CH}_4$ , (2) the presence of infinite amounts of  $\text{CH}_4$  ice at the equator (BTD), which continuously feed the atmosphere with gaseous  $\text{CH}_4$ . Indeed, the BTD are found to be a net sublimation zone of  $\text{CH}_4$  ice over astronomical timescales, transporting  $\text{CH}_4$  ice to the mid-to-polar regions. As shown in Table 2 and Figure 4,  $\sim 90$  m of  $\text{CH}_4$  ice are lost by the BTD and 30 m of  $\text{CH}_4$  ice accumulated between  $30^\circ\text{N}$ - $60^\circ$  after 30 Myrs.

We performed the same simulations but starting at  $t_0 = -100, -200$  and  $-300$  Myrs, in order to verify if the transport of  $\text{CH}_4$  ice from the BTD to the mid-latitudes also occurs in different configuration for Pluto's orbit (the entire period of the cycle obliquity + solar longitude of perihelion at maximum obliquity is 375 Myrs, as shown in Figure 5 in B2018). We obtained similar results. Consequently, assuming that the Milankovitch cycles on Pluto remain stable with time, if we let this simulation evolve over 1 billion years, 3 km of  $\text{CH}_4$  ice would have been transferred from the BTD to the mid-latitudes, where  $\text{CH}_4$  ice would form a 1 km thick mantle. These results are consistent with the observations of New Horizons showing that the mid-latitudes are covered by a kilometer-thick mantle of volatile ice (Howard et al., 2017). They suggest that  $\text{CH}_4$  has been accumulated there since hundreds of Myrs by the action of  $\text{N}_2$  condensation-sublimation, and that the BTD have been losing significant amounts of  $\text{CH}_4$  ice by sublimation. We further discuss this point in Section 5.

#### 4.2.2 The current seasonal cycle of $\text{CH}_4$

Figure 4 shows that, at astronomical scale, present-time Pluto is in a period of its Milankovitch cycle where  $\text{N}_2$  and  $\text{CH}_4$  perennial deposits are not favored at high latitudes, compared to other periods (such as 2 Myrs ago for instance). Figure 5 shows the latitudinal distribution of  $\text{N}_2$  (in blue, mixed with  $\text{CH}_4$ ) and  $\text{CH}_4$  (in red, no  $\text{N}_2$ ) ice obtained over a current Pluto year and after 30 Myrs of simulation.

In the northern hemisphere, we can distinguish three different regions in latitudes.

- (1) Around the North Pole (above  $75^\circ\text{N}$ ),  $\text{CH}_4$  condenses as a thin frost ( $< 1$  mm) during fall and triggers the condensation of  $\text{N}_2$  ice on it during winter. When spring begins (Earth year 1988), the thin  $\text{N}_2$  deposit

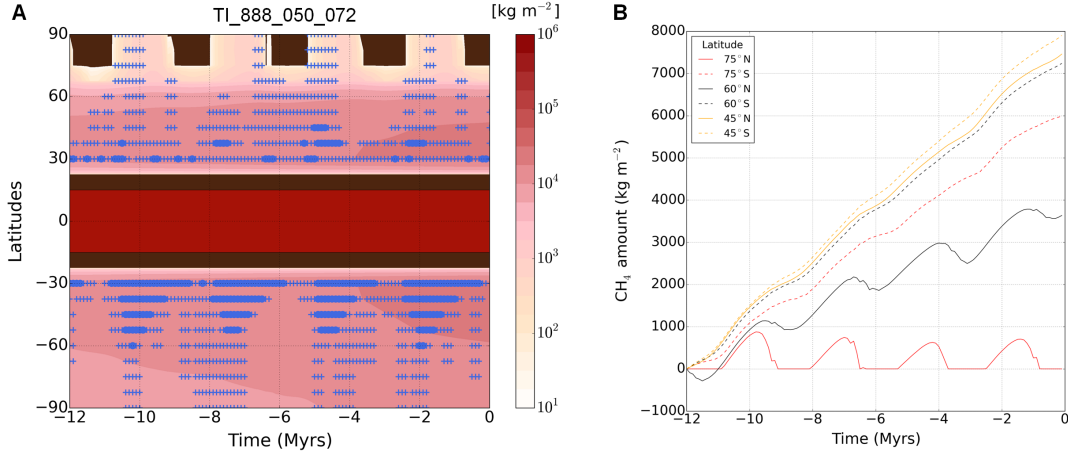


Fig. 4. Simulation #TI888\_050\_072. A. Evolution of the perennial  $\text{CH}_4$  ice deposits: minimum amount of surface  $\text{CH}_4$  ice (per Pluto year, over the last 12 millions of Earth years, that is  $\sim 4$  obliquity cycles). Seasonal deposits (frosts) are not shown. The dark-red band at the equator indicates the latitudes of the modeled BTD, which are an infinite source of  $\text{CH}_4$  in the simulations. The dark-brown color represents the dark, tholin-covered bedrock. The blue markers (cross and star) indicate the presence of  $\text{N}_2$  ice perennial deposits, which are obtained at low elevations only (patchy deposits: cross) or over all longitudes (latitudinal band: star). B. Variation of the amount of surface  $\text{CH}_4$  ice as shown in the panel A, for different latitudes and normalized at  $t = -12$  Myrs. At the northern polar latitudes, perennial deposits form and disappear at each astronomical cycle.

(< 1 cm) starts to sublime. It disappears around year 2000, revealing a bright thin  $\text{CH}_4$  frost that will last until 2017 before disappearing and leaving the dark substrate volatile-free during the entire summer. This is consistent with Figure 4.A, which predicts that there is no perennial deposit at the North Pole for the current epoch.

- (2) At mid-latitudes ( $45^\circ\text{N}$ - $75^\circ\text{N}$ ), seasonal 1-m thick  $\text{N}_2$  ice deposits cover  $\text{CH}_4$  ice during most of the year, except during late spring and summer. During this period,  $\text{N}_2$  ice sublimates from the pole and reveals the  $\text{CH}_4$  ice mantle which starts to sublime as well. However, over the entire Pluto year, there is a net accumulation of  $\text{CH}_4$  ice at these latitudes, leading to the formation of a thick mantle of  $\text{CH}_4$  ice over Myrs, as shown in Figure 4.A.
- (3) Between  $30^\circ\text{N}$ - $45^\circ\text{N}$ , a perennial latitudinal band of  $\text{N}_2$  ice is obtained.

The southern hemisphere is covered by up to 1 m thick  $\text{N}_2$  ice deposits during most of the year except during late summer, where it sublimates from the pole and reveals the  $\text{CH}_4$  ice mantle. Around 1988, when southern fall begins,  $\text{N}_2$  ice condenses and first covers the South Pole and then the mid-latitudes. A net accumulation of  $\text{CH}_4$  ice occurs in the southern hemisphere over seasonal and astronomical timescales.

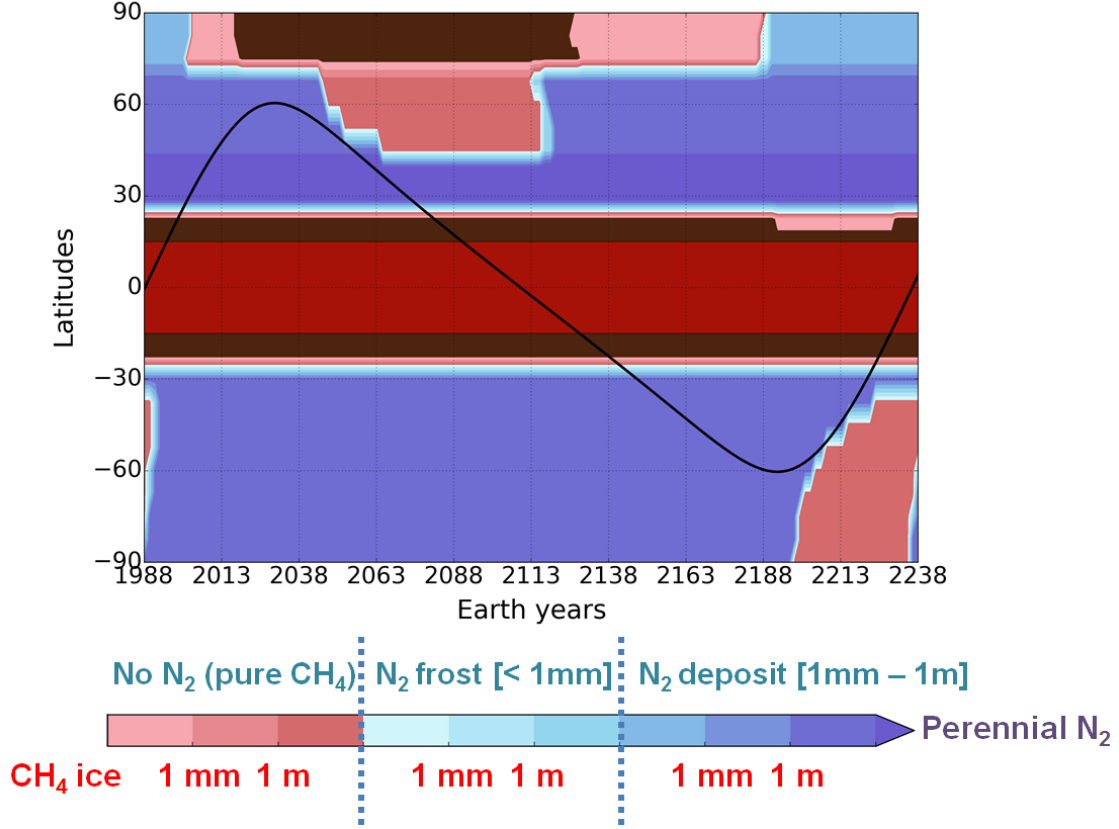


Fig. 5. Reference simulation #TI888\_050\_072. Evolution of the latitudinal distribution of the deposits over a current annual timescale (at longitude  $0^\circ$ ). The solid dark line shows the position of the subsolar point with time. Blue colors indicate the presence of  $N_2$  ice and  $CH_4$  ice while red colors indicate the presence of  $CH_4$  ice only. The lighter the color, the thinner is the deposit. The dark-red band at the equator indicates the latitudes of the modeled BTM, which are an infinite source of  $CH_4$  in the simulations. The dark-brown color represents the dark, tholin-covered bedrock.

#### 4.3 Sensitivity to the albedo of the equatorial $CH_4$ deposits

Three different scenarios are obtained in our simulations if we increase or decrease the albedo of the modeled BTM ( $A_{CH_4eq}$ ):

- (1) If  $A_{CH_4eq} \ll 0.6$ , the BTM are dark and warm enough so that they never trigger  $N_2$  condensation. Lower albedo values lead to enhanced sublimation rates of  $CH_4$  above these deposits and larger amounts of  $CH_4$  ice transported to the mid-to-polar regions. For instance, Figure 6 shows the results obtained from simulation #TI888\_030\_072, performed with an equatorial  $CH_4$  albedo of 0.3. In this simulation, up to 1 km of  $CH_4$

ice has been lost from the BTB after 30 Myrs (Table 2), and transported to the mid-to-polar regions. In this case,  $\text{CH}_4$  is able to remain around the north pole and form perennial deposits at all times.

- (2) If  $A_{\text{CH}_4\text{eq}} \approx 0.6$ , condensation of  $\text{N}_2$  occurs on the  $\text{CH}_4$  equatorial deposits but only at low elevations (simulations #TI888\_060\_072, #TI888\_060\_080, #TI888\_065\_072, #TI888\_065\_080). The case of #TI888\_065\_072 is shown in Figure 7. Up to 200-300 m thick  $\text{N}_2$  ice deposits form in the low-elevated equatorial regions where  $\text{CH}_4$  ice is present (see blue-star markers on Figure 7.A and  $\text{Max}_{\text{eqN}_2}$  in Table 2). The high altitude BTB remain  $\text{N}_2$ -free and feed the atmosphere with gaseous  $\text{CH}_4$  as they sublime, allowing the formation of perennial and seasonal  $\text{CH}_4$  deposits at the poles. These mid-to-polar deposits are thinner than in the reference case because part of the equatorial source of gaseous  $\text{CH}_4$  is trapped by  $\text{N}_2$  ice.
- (3) If  $A_{\text{CH}_4\text{eq}} \gg 0.6$ , then the BTB are bright enough to trigger  $\text{N}_2$  condensation at most altitudes. They are covered and cold trapped by 200-300 m of  $\text{N}_2$  ice (see Table 2), mostly in the low-elevated regions since this is enough  $\text{N}_2$  to flow downhill. These  $\text{N}_2$  deposits remain relatively stable at such equatorial latitudes, as demonstrated by B2018 as well. In this case, the  $\text{CH}_4$  sublimation at the equator is limited and thus there is not enough gaseous  $\text{CH}_4$  available to form mid-to-polar deposits. As a result, Pluto's surface outside the equatorial regions remains volatile-free, which is not realistic (no simulation result is shown for this case).

To summarize, Table 2 shows that the amount of  $\text{CH}_4$  ice lost by the modeled BTB over 30 Myrs is about 1 m, 10 m, 100 m or 1000 m assuming a  $\text{CH}_4$  ice albedo of 0.65, 0.6, 0.5, or 0.3 respectively.

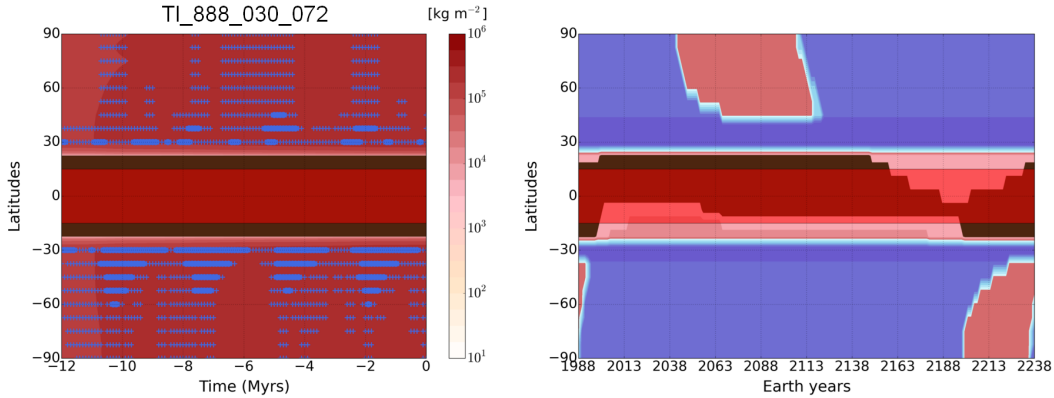


Fig. 6. Simulation #TI888\_030\_072. Same as Figure 4 and Figure 5 (legends are the same), except for an equatorial  $\text{CH}_4$  ice albedo of 0.3 (very dark BTB).

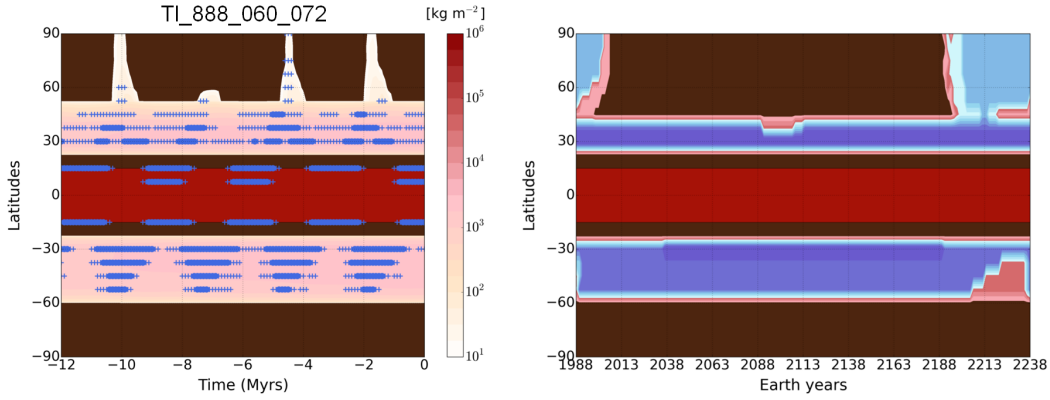


Fig. 7. Simulation #TI888\_060\_072. Same as Figure 4 and Figure 5, except for an equatorial  $\text{CH}_4$  ice albedo of 0.60 (relatively bright BTB).

#### 4.4 Sensitivity to the albedo of the mid-to-polar $\text{CH}_4$ deposits

Our results are also very sensitive to the albedo of the mid-to-polar  $\text{CH}_4$  ice deposits. When this albedo is higher than 0.6,  $\text{N}_2$  ice tends to condense on the  $\text{CH}_4$  ice during fall-winter and form seasonal (few mm thick) or perennial deposits (up to 20 m thick), as shown for the reference case by Figure 4 and Figure 5. If the mid-to-polar  $\text{CH}_4$  ice albedo is lower than 0.6, then only thin seasonal frosts of  $\text{CH}_4$  are obtained at the poles during fall-winter, as they do not trigger  $\text{N}_2$  condensation. This case corresponds to the results obtained in Section 3 and in BF2016.

The higher the albedo of mid-to-polar  $\text{CH}_4$  ice, the more  $\text{N}_2$  condenses, at higher latitudes, and the longer it remains and traps  $\text{CH}_4$  during Pluto's year. For instance, in our simulation using a mid-to-polar  $\text{CH}_4$  ice albedo of 0.65 (#TI888.050\_065, Figure 8), we obtain perennial  $\text{N}_2$  deposits at  $30^\circ\text{N}$  and very thin seasonal  $\text{N}_2$  deposits at higher latitudes and in the southern hemisphere above  $50^\circ\text{S}$ . As a result,  $\text{CH}_4$  ice does not form thick deposits outside  $50^\circ\text{N}$ - $50^\circ\text{S}$ , but only seasonal frosts (e.g. the northern polar frost quickly disappears after 2013).

This is to be compared with the reference simulation (Figure 4 and Figure 5), where the brighter mid-to-polar  $\text{CH}_4$  ice albedo (0.72) triggers  $\text{N}_2$  condensation at higher latitudes and leads to thick  $\text{CH}_4$  ice deposits up to  $70^\circ\text{N}$  and  $90^\circ\text{S}$ , while the northern polar frost quickly disappears after 2017.

Finally, in the more extreme case of a mid-to-polar ice albedo of 0.8 (#TI888.050\_080, Figure 9), perennial deposits of  $\text{N}_2$  ice extend up to the pole during half of an

obliquity cycle. During the current-year Pluto,  $N_2$  ice covers the bright  $CH_4$  ice up to the poles during most of the year, except during a short period in summer. In this simulation, long term accumulation of  $CH_4$  ice is obtained everywhere outside the equatorial regions.

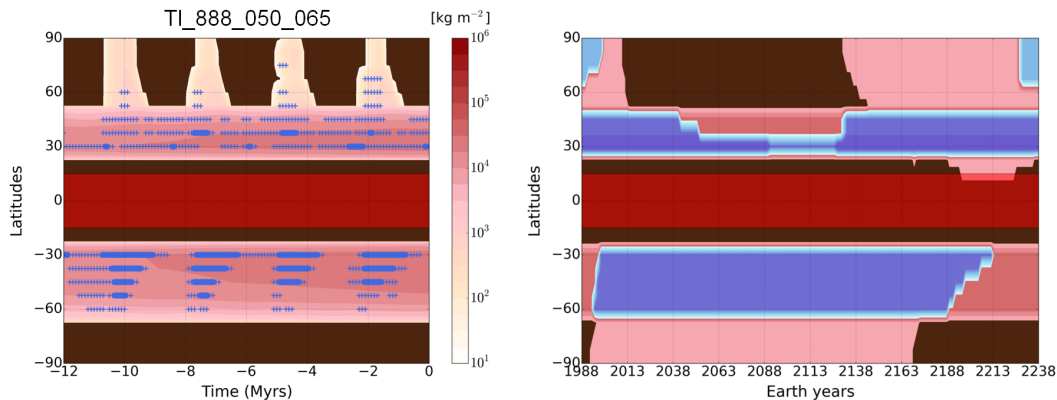


Fig. 8. Simulation #TI888\_050\_065. Same as Figure 4 and Figure 5, except for a mid-to-polar  $CH_4$  ice albedo of 0.65.

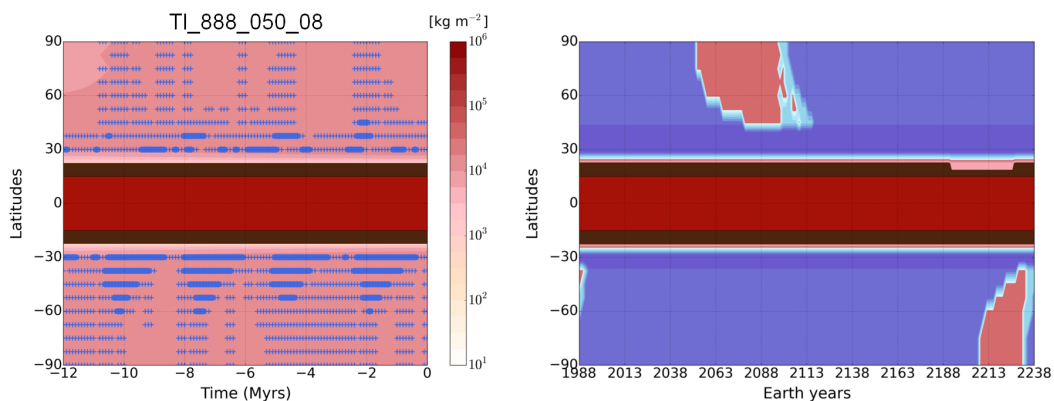


Fig. 9. Simulation #TI888\_050\_080. Same as Figure 4 and Figure 5, except for a mid-to-polar  $CH_4$  ice albedo of 0.8.

#### 4.5 Sensitivity to $N_2$ ice phase emissivity

The emissivity of  $N_2$  ice in its  $\alpha$ -phase is less than that in its  $\beta$ -phase (Stansberry and Yelle, 1999; Lellouch et al., 2011b). Here we tested the sensitivity of the results to the  $N_2$  ice emissivity by assuming that it varies between  $\varepsilon_\alpha=0.3$  in  $\alpha$ -phase and  $\varepsilon_\beta=0.8$  in  $\beta$ -phase, as described in Section 2.3. This assumption

has a strong impact on the  $N_2$  cycle because the change of emissivity forces the ice surface temperature to remain at the transition temperature  $T_{\alpha-\beta}=35.6$  K during most of Pluto's northern fall and winter. Consequently, higher annual mean  $N_2$  ice surface temperature and surface pressure are obtained.

Figure 10 shows the results obtained for simulation #TI888\_050\_072\_phase, which reproduces the reference simulation but taking into account the change of  $N_2$  ice emissivity. The main differences with the results from the reference simulation (Figure 4 and Figure 5) are: (1)  $N_2$  ice does not form thick perennial deposits outside Sputnik Planitia. Over a current annual timescale,  $N_2$  ice deposits in the mid-to-polar regions are only seasonal and disappear during summer. In the last 12 Myrs, perennial deposits are obtained only at low elevations, (2) No  $N_2$  ice forms at the south pole during a current Pluto year, (3)  $CH_4$  ice does not accumulate above  $50^\circ N$  and below  $70^\circ S$ .

Consequently, the decrease of  $N_2$  ice emissivity with temperature is an example of negative feedback which would limit the formation of  $N_2$  deposits outside Sputnik Planitia.

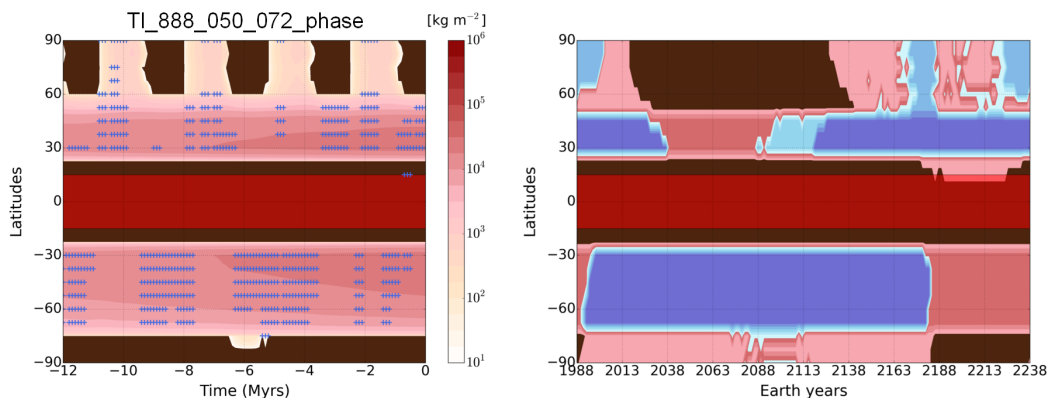


Fig. 10. Simulation #TI888\_050\_072\_phase. Same as Figure 4 and Figure 5, except that the  $N_2$  ice emissivity varies according to its phase ( $\alpha$  or  $\beta$ ) from  $\varepsilon_\alpha=0.3$  to  $\varepsilon_\beta=0.8$ .

#### 4.6 Sensitivity to the thermal inertia of the different ices

In the previous sections, simulations have been performed assuming a global uniform thermal inertia. In reality, the ices have different thermal inertia as it depends on the porosity of the material, the size of grains (larger grains lead to higher thermal inertia)... In this section, we allow each ice to have its own TI in the model, ranging from 400 SI to 1200 SI, and we explore the impact



of these changes on the results (summarized in the second part of Table 2).

For instance, simulation #TI8412.050\_065 has been performed with a thermal inertia of 800 SI for  $\text{N}_2$  ice (8), 400 SI for  $\text{CH}_4$  ice (4) and 1200 SI (12) for the water ice bedrock. In the model, TI evolves with time depending on the new thickness of the volatile ice on Pluto’s surface. If a 1 m thick layer of  $\text{CH}_4$  ice lies on water ice in the model, then the TI is set to 400 SI over the first meter of the subsurface and to 1200 SI below (in practice in the model the conductivity is modified to correspond to the required thermal inertia).

Changing the TI of  $\text{N}_2$  ice (e.g. simulations #TI488 or #TI1288) does not significantly change the ice distribution. This is because to first order, the variation of the exchanged mass of  $\text{N}_2$  between the surface and the atmosphere is independent of thermal inertia, as detailed in Section 2.2 in B2018.

Changing the TI of  $\text{CH}_4$  ice has also little impact on the ices distribution. Lower values of TI allows for colder  $\text{CH}_4$  ice during winter, and eventually to slightly larger seasonal and perennial reservoirs of  $\text{N}_2$  ice at the poles (simulations #TI848, #TI8412). The impact is also limited by the fact that the simulated  $\text{CH}_4$  ice deposits are thin (few meter thick), because the initial reservoir is low (see Section 2.4).

Changing the TI of water ice has a significant impact on the thin volatile ice deposits, and therefore mostly at the poles. Low TI allows colder poles in winter and the formation of thicker  $\text{CH}_4$  and  $\text{N}_2$  deposits there (simulations #TI884). For instance, in the case of a mid-to-polar  $\text{CH}_4$  ice albedo of 0.65 (#TI884.05\_065, Figure 11), the northern polar  $\text{N}_2$  deposit remains until years 2015-2020, and the  $\text{CH}_4$  frost until 2025. This is to be compared with simulation #TI888.05\_065 (Figure 8), where the northern frosts only last until 2000 and 2010 respectively, and where no  $\text{N}_2$  condenses at the south pole. The effect is even stronger if we compare #TI884.05\_072 (Figure 13) with the reference case TI888.05\_072 (Figure 5). The  $\text{N}_2$  polar deposit remains longer in northern spring and disappears after 2038, while the polar frost of  $\text{CH}_4$  remains during the entire Pluto year.

To summarize, our results are much less sensitive to TI (in the range 400-1200 SI) than albedos, although the TI of the water ice bedrock significantly impacts the distribution of the thin polar deposits.

#### 4.7 *Summary of simulation results*

Figure 15 gives an overview of the different simulations performed in this Section 4 and the different ices distributions obtained depending on the assumed albedo for  $\text{CH}_4$  ice. Figure 15.1 shows how the simulations were initialized:

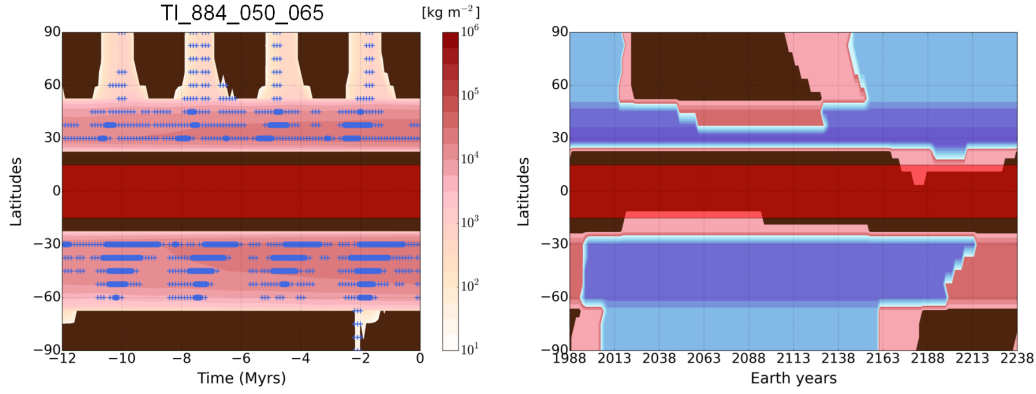


Fig. 11. Simulation #TI884\_050\_065. Same as Figure 4 and Figure 5, except for a mid-to-polar  $\text{CH}_4$  ice albedo of 0.65 and a TI for water ice of 400 SI.

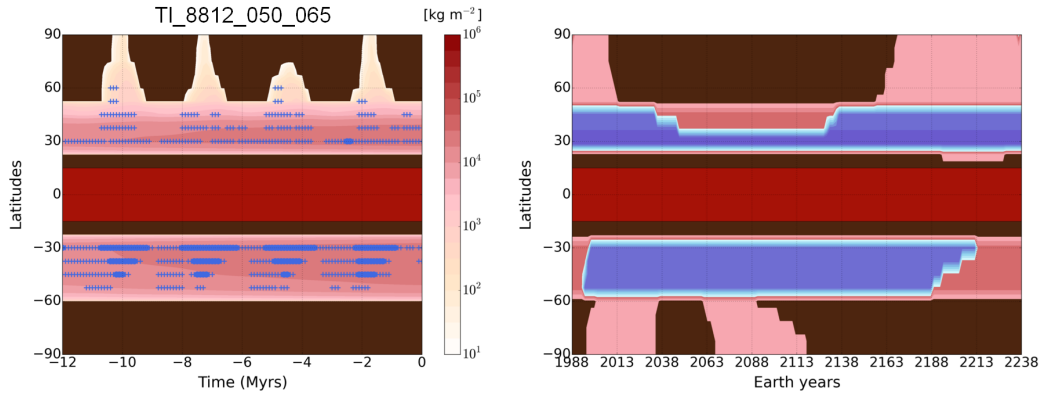


Fig. 12. Simulation #TI8812\_050\_065. Same as Figure 4 and Figure 5, except for a mid-to-polar  $\text{CH}_4$  ice albedo of 0.65 and a TI for water ice of 1200 SI.

$\text{N}_2$  ice fills Sputnik Planitia while unlimited amounts of  $\text{CH}_4$  ice are placed roughly at the location of the BTB. If the  $\text{CH}_4$  ice albedo remains well below 0.6, only seasonal  $\text{CH}_4$  frosts form at the poles, as shown in Figure 15.2. If the modeled BTB have an albedo well above 0.6 (Figure 15.3), then they become cold enough to trigger  $\text{N}_2$  condensation. The  $\text{N}_2$  ice deposits thus formed trap the  $\text{CH}_4$  ice, which cannot feed the atmosphere with gaseous  $\text{CH}_4$ . As a result, there is no gaseous  $\text{CH}_4$  left in the system and no frost can form at the poles, which remain volatile-free at all times. Using an albedo for the BTB around 0.6 allows the formation of  $\text{N}_2$  ice deposits only in the depressions of these terrains, as shown in Figure 15.4. The high-altitude BTB remains  $\text{N}_2$ -free and feed the system with  $\text{CH}_4$ , allowing the formation of seasonal frosts at the

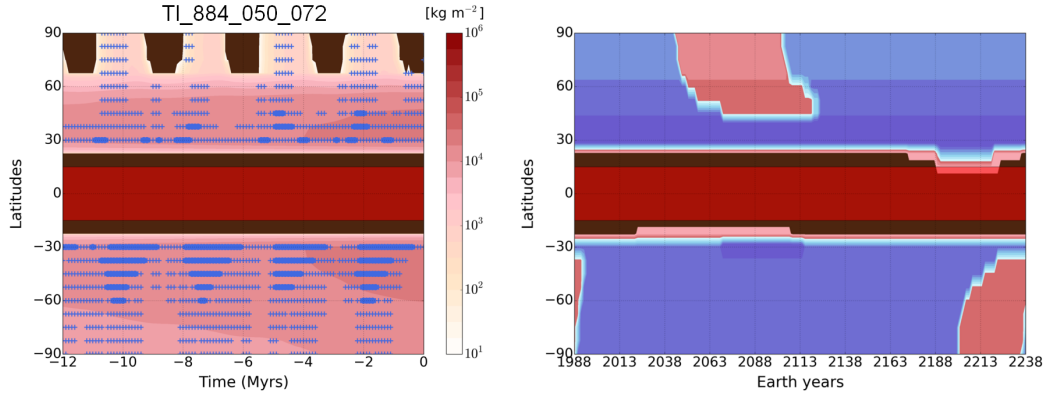


Fig. 13. Simulation #TI884\_050\_072. Same as Figure 4 and Figure 5, except for a TI for water ice of 400 SI.

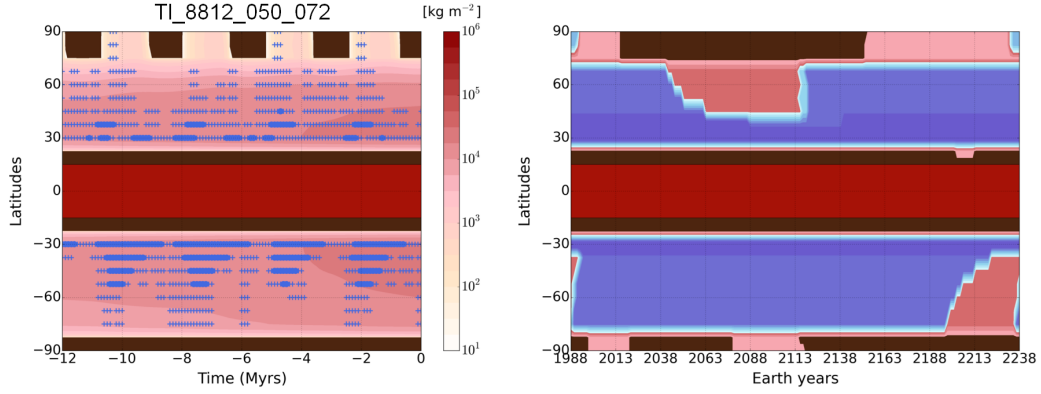


Fig. 14. Simulation #TI8812\_050\_072. Same as Figure 4 and Figure 5, except for a TI for water ice of 1200 SI.

poles. Finally, if the albedo of the mid-to-polar  $\text{CH}_4$  deposits is set higher than 0.6 (Figure 15.5), then  $\text{N}_2$  can condense and form thin seasonal deposits at the poles and larger deposits at mid-latitudes, which can be perennial or seasonal (up to few tens of meter thick, in particular in depressions). These  $\text{N}_2$  deposits are able to trap large amounts of  $\text{CH}_4$  ice, resulting in the formation of a thick mid-latitudinal mantle of  $\text{CH}_4$  ice.

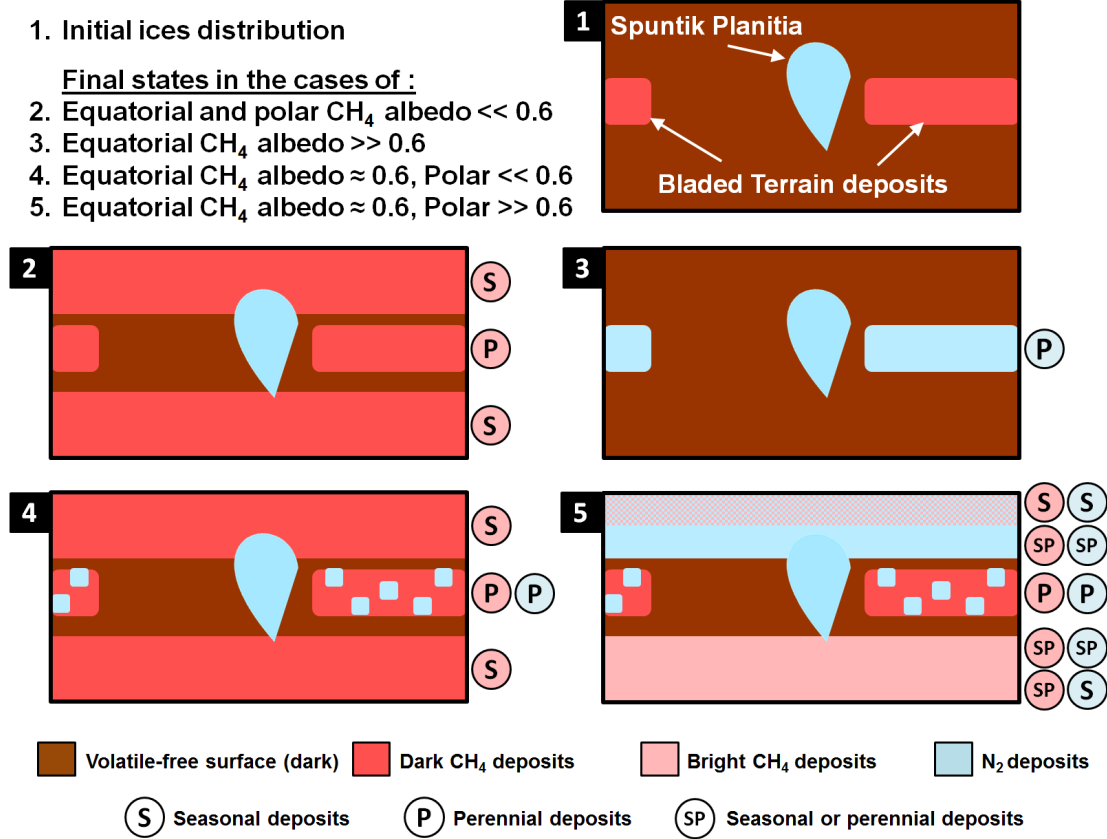


Fig. 15. Summary of the simulation obtained in Section 4.

#### 4.8 Surface pressure and $\text{CH}_4$ atmospheric mixing ratio

##### 4.8.1 The peak surface pressure during northern spring

Simulations from BF2016 predicted an evolution of surface pressure in accordance with the stellar occultation observations conducted from Earth since 1988. The threefold increase of pressure observed would result from  $\text{N}_2$  ice heating when (1) Sputnik Planitia is most exposed to sunlight (shortly after the northern spring equinox in 1989) and (2) Pluto is close to the Sun. Their model also predicts that the atmospheric pressure should decrease in the following decades, after reaching its maximum around 2015, because of the orbitally-driven decline of insolation above Sputnik Planitia.

Here, in this paper, although the general aspect of the annual evolution of surface pressure remains unchanged (see Figure 2.a in BF2016), the peak surface pressure occurs earlier than 2015 in many of our simulations. The main differences between the simulations of this paper and those from BF2016 are the presence of  $\text{N}_2$  ice deposits outside Sputnik Planitia that slightly affect the evolution of pressure (by enhancing the global condensation or sublimation

flow) and the better resolution of the Sputnik Planitia basin (BF2016 only assumed a circular crater).

Our simulations show that the annual pressure peak occurs when the area of the sublimation source in the northern hemisphere becomes less than the area of the condensation sink in the southern hemisphere. For instance, in the reference simulation (#TI888\_050\_072), the peak occurs in year 2000 when the northern polar deposit of  $N_2$  disappears.

Simulations with a peak surface pressure occurring after 2010 are (1) the ones with a very high mid-to-polar  $CH_4$  albedo, leading to both hemispheres covered by  $N_2$  ice during northern spring (these cases are not realistic because they do not correspond to the ice distribution observed by New Horizons), (2) the ones with a thermal inertia for water ice around 400 SI (#TI444, #TI884, #TI12124). In these cases, the thin northern polar deposit of  $N_2$  lasts until 2010-2015, (3) The ones without  $N_2$  ice outside SP (like in BF2016). This scenario is only obtained when using in the model a dark mid-to-polar  $CH_4$  albedo (less than 0.6).

These results suggest that the southern hemisphere of Pluto is not entirely covered by  $N_2$ -rich ice, otherwise the peak surface pressure would have occurred much earlier than 2015 (a similar result is found in [Young \(2013\)](#); [Olkin et al. \(2015\)](#)). At most, a thin mid-latitude band of  $N_2$ -rich ice (similar to that observed in the northern hemisphere) could be present in the southern hemisphere in 2015.

#### *4.8.2 Evolution of surface pressure over astronomical timescales*

In all simulations of this paper, the surface pressure obtained remains within few mPa-Pa, with a maximal value of 4 Pa over 30 Myrs. This is in the same range than the values obtained in B2018 (see Figure 16 of their paper, lines obtained with an albedo of 0.7 for  $N_2$  ice). We could have expected higher values in the results of this paper because we obtained  $N_2$  deposits at the poles. However, the increase of pressure due to their sublimation in summer is always balanced by the strong condensation flux at the opposite pole.

#### *4.8.3 Evolution of $CH_4$ atmospheric mixing ratio over astronomical timescales*

The atmospheric mixing ratio of  $CH_4$  obtained is very sensitive to model parameters ([Bertrand and Forget, 2016](#)), in particular those controlling the BTD (main source of gaseous  $CH_4$ ). Figure 16 shows the annual maximum and minimum values obtained over astronomical timescales for different simulations. We note that (1) The  $CH_4$  atmospheric mixing ratio remains within 0.001-1% in most of the simulations, including the reference case, (2) Higher values

can be obtained for a lower equatorial  $\text{CH}_4$  albedo (0.01-10% with an albedo of 0.3), (3) Lower values are obtained when  $\text{N}_2$  condenses on the equatorial  $\text{CH}_4$  deposits ( $10^{-4}$ - $10^{-2}\%$ ), (4) The lower the albedo of the mid-to-polar  $\text{CH}_4$  deposits, the higher the concentration of  $\text{CH}_4$  in the atmosphere (because of the higher equilibrium temperature and pressure of  $\text{CH}_4$  and because there is less  $\text{N}_2$  deposit forming and therefore more  $\text{CH}_4$  ice available to feed the atmosphere with gaseous  $\text{CH}_4$ ).

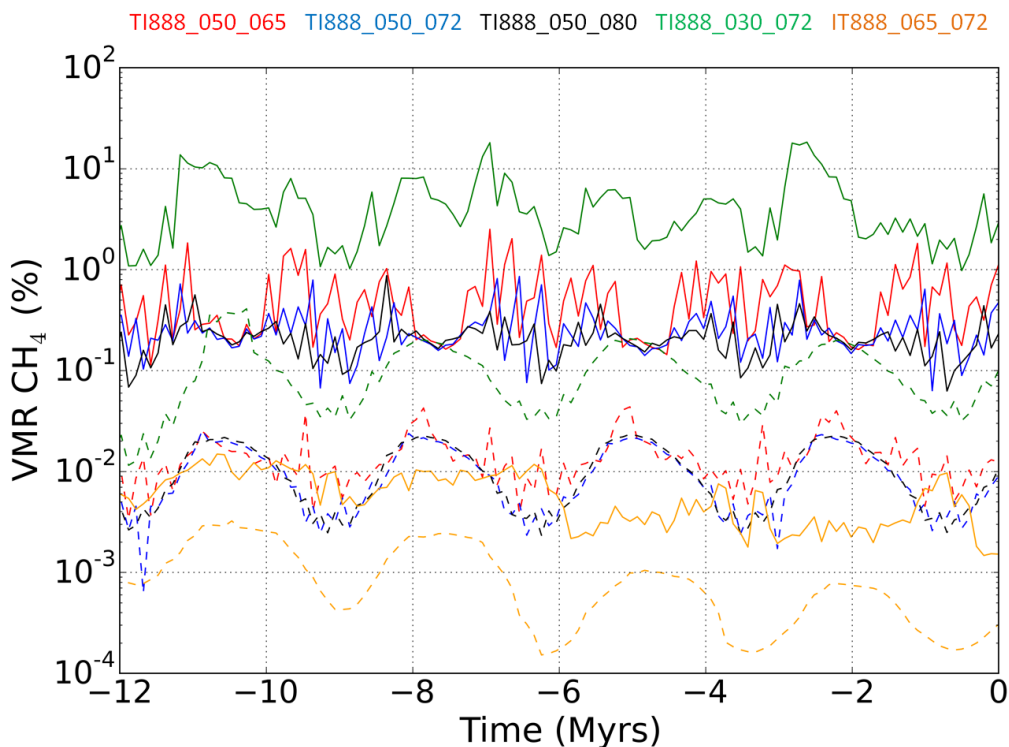


Fig. 16. Evolution of the annual maximum (solid line) and minimum (dashed line) global mean atmospheric mixing ratio of  $\text{CH}_4$  for different simulations of this paper.

#### 4.8.4 Opacity of Pluto's atmosphere at Lyman- $\alpha$ wavelengths

On Pluto, solar ultraviolet light is dominated by Lyman- $\alpha$  photons, which control much of the photodissociation of  $\text{CH}_4$  and of the subsequent hydrocarbon photochemistry (Gladstone et al., 2016; Grundy et al., 2018). Bertrand and Forget (2017) showed that the photochemical reactions are photon-limited in present-day Pluto's atmosphere, i.e. that enough gaseous  $\text{CH}_4$  is present for all photons to be absorbed by  $\text{CH}_4$  molecules.

Here we want to assess the opacity of Pluto's atmosphere at Lyman- $\alpha$  wavelengths over astronomical timescales. Indeed, if the atmospheric mixing ratio of  $\text{CH}_4$  or the entire atmosphere collapsed in Pluto's past, then a direct photolysis of surface ices and tholins could have happened, which would help

understanding the high degree of processing of the dark material in Cthulhu (Grundy et al., 2018).

To do that, we first estimate the total incident flux of Lyman- $\alpha$  at Pluto over one orbit ( $F_{tot}$ ), considering the solar as well as the interplanetary medium (IPM) Lyman- $\alpha$  sources (Gladstone et al., 2015), as given by Eq. 2 and Eq. 5 in Bertrand and Forget (2017):

$$F_{tot}(d_p) = \frac{F_{Earth}}{4d_p^2} * 0.875 + F_{IPM} \quad (2)$$

We assume a constant solar Lyman- $\alpha$  flux at Earth  $F_{Earth}=4 \times 10^{15} \text{ ph m}^{-2} \text{ s}^{-1}$ , a constant IPM flux at Pluto  $F_{IPM}=7.25 \times 10^{11} \text{ ph m}^{-2} \text{ s}^{-1}$  and a constant extinction factor of 0.875. The IPM flux does not strongly depend on the Sun-Pluto distance  $d_p$  (Gladstone et al., 2015), therefore we consider it constant over time. The integration of  $F_{tot}$  over one Pluto orbit gives an annual mean incident Lyman- $\alpha$  flux of  $1.3 \times 10^{12} \text{ ph m}^{-2} \text{ s}^{-1}$ . We then use Eq. 1 in B2018 to estimate the fraction of this incident Lyman- $\alpha$  flux reaching the surface (Beers law), by feeding this equation with the values of surface pressure and atmospheric  $\text{CH}_4$  mixing ratio obtained from our simulations over 30 Myrs.

Figure 17 shows the results for the same simulations than those shown on Figure 16. The atmosphere remains relatively opaque at Lyman- $\alpha$  wavelengths over astronomical timescales. For the most realistic simulations, the fraction of the annual mean incident flux that reaches the surface varies between 0.01 and 10% over time, with the lowest values obtained during high-obliquity periods, when mid-to-polar  $\text{N}_2$  ice deposits are less stable. Over a current-year Pluto, we estimate that the fraction of Lyman- $\alpha$  reaching Pluto’s surface is less than 1% of the total flux received. These fractions of Lyman- $\alpha$  flux may be sufficient to have a significant effect on the chemistry of the  $\text{N}_2:\text{CH}_4:\text{CO}$  ice mixtures (Materese et al., 2015; Grundy et al., 2018). Indeed, even if most of the Lyman- $\alpha$  flux is greatly attenuated most of the time, the photolysis of the ices goes on, albeit more slowly.

The fraction becomes negligible when the atmosphere is enriched in gaseous  $\text{CH}_4$ , as it is the case if a low albedo of the equatorial  $\text{CH}_4$  deposits is considered (#TI888\_030\_072, green line). However, most of the incident flux can reach the surface if the atmospheric  $\text{CH}_4$  mixing ratio is less than 0.01% over an entire year, as it is the case for the simulations where  $\text{N}_2$  covers the equatorial  $\text{CH}_4$  deposits (#TI888\_065\_072, orange line). In this case, the  $\text{CH}_4$  cycle is disrupted because the sources of gaseous  $\text{CH}_4$  are trapped by  $\text{N}_2$  ice, and  $\text{CH}_4$  can no longer block the energetic radiation, which would act directly on Pluto’s surface ices.

Table 2. Settings and results of the simulations performed from 30 Myrs ago to present-day. From left to right, settings are: Run name (\* indicates that the run is illustrated by figures in this paper), thermal inertia of N<sub>2</sub>, CH<sub>4</sub>, H<sub>2</sub>O ice, equatorial and mid-to-polar CH<sub>4</sub> albedo. Results are: Loss of equatorial CH<sub>4</sub> ice after 30 Myrs, year of maximum pressure in current epoch, latitudes between which perennial N<sub>2</sub> ice deposits (pN<sub>2</sub>) are obtained in the northern hemisphere, maximal thickness of these perennial deposits, same for seasonal deposits (sN<sub>2</sub>), and maximal thickness of the equatorial N<sub>2</sub> ice deposits (formed on the modeled LTD).

Name	T <sub>N<sub>2</sub></sub>	T <sub>CH<sub>4</sub></sub> (J s <sup>-1/2</sup> m <sup>-2</sup> K <sup>-1</sup> )	T <sub>H<sub>2</sub>O</sub>	A <sub>CH<sub>4</sub> eq</sub>	A <sub>CH<sub>4</sub> poles</sub>	L <sub>CH<sub>4</sub></sub> (m)	Y <sub>p</sub>	Lat <sub>p</sub> N <sub>2</sub> (°)	Max <sub>p</sub> N <sub>2</sub> (m)	Lat <sub>s</sub> N <sub>2</sub> (°)	Max <sub>s</sub> N <sub>2</sub> (m)	Max <sub>eq</sub> N <sub>2</sub> (m)
#T1888.050.060	800	800	800	0.5	0.65	75	1998.6	30	1.5	30-90	0.35	0
#T1888.050.067*	800	800	800	0.5	0.65	87	1996.9	30	1.5	37.5-90	0.51	0
#T1888.050.068	800	800	800	0.5	0.68	88	1995.1	30	4.0	37.5-90	0.59	0
#T1888.050.072*	800	800	800	0.5	0.72	91	2000.4	30-37.5	4.9	45-90	0.75	0
#T1888.050.080*	800	800	800	0.5	0.8	92	2017.9	30-37.5	7.3	45-90	0.90	0
#T1888.050.065	800	800	800	0.5	0.65	72	2000.4	30-37.5	7.3	45-90	0.08	0
#T1888.050.072	800	800	800	0.5	0.72	86	1998.6	30-37.5	3.2	30-90	0.34	0
#T1888.050.080	800	800	800	0.5	0.8	88	2017.9	30-37.5	3.2	30-90	0.77	0
#T1888.050.072_phase*	800	800	800	0.5	0.72	174	2016.9	30-37.5	8.6	45-90	0.74	0
#T1888.030.065	800	800	800	0.3	0.72	174	2016.9	30-37.5	8.6	45-90	0.74	0
#T1888.060.072*	800	800	800	0.6	0.72	174	2016.9	30-37.5	8.6	45-90	0.74	0
#T1888.060.072	800	800	800	0.6	0.8	10	1996.9	30-37.5	4.9	45-90	0.66	77
#T1888.065.072	800	800	800	0.65	0.72	3	2002.1	30-37.5	7.7	45-90	0.86	357
#T1888.065.080	800	800	800	0.65	0.8	1	1996.9	30-37.5	4.7	45-90	0.68	185
#T1884.050.065*	800	800	400	0.5	0.65	85	2014.4	30	10.5	22.5-90	0.51	0
#T1884.050.072*	800	800	400	0.5	0.72	90	2019.6	30-37.5	6.2	22.5-90	0.81	0
#T18812.050.065*	800	800	1200	0.5	0.65	85	1995.1	30	3.8	37.5-90	0.44	0
#T18812.050.072*	800	800	1200	0.5	0.72	91	2014.4	30-37.5	14.6	45-90	0.70	0
#T1848.050.065	800	400	800	0.5	0.65	106	1996.9	30	5.5	37.5-90	0.58	78
#T1848.050.072	800	400	800	0.5	0.72	106	2003.6	30-37.5	9.4	45-90	0.78	72
#T18128.050.065	800	1200	800	0.5	0.72	77	1998.6	30	1.0	37.5-90	0.71	0
#T18128.050.072	800	1200	800	0.5	0.72	77	1998.6	30	1.0	37.5-90	0.71	0
#T1488.050.065	400	800	800	0.5	0.65	86	1995.1	30	2.4	45-90	0.51	0
#T1488.050.072	400	800	800	0.5	0.72	90	2002.1	30-37.5	5.5	45-90	0.77	0
#T11288.050.065	1200	800	800	0.5	0.65	87	1995.1	30	2.8	37.5-90	0.57	0
#T11288.050.072	1200	800	800	0.5	0.72	92	2000.4	30-37.5	6.2	45-90	0.74	0
#T1444.050.072	400	400	400	0.5	0.72	105	2010.9	30-37.5	8.3	22.5-90	0.77	91
#T1444.050.080	400	400	400	0.5	0.8	105	2016.1	30-37.5	6.7	22.5-90	0.93	105
#T1844.050.060	800	400	400	0.5	0.65	105	2010.9	30	7.3	22.5-90	0.46	22
#T1844.050.072	800	400	400	0.5	0.72	108	2014.4	30	10.2	22.5-90	0.70	82
#T1844.050.075	800	400	400	0.5	0.75	108	2014.4	30	10.2	22.5-90	0.70	82
#T18412.050.065	800	400	1200	0.5	0.65	133	1996.9	30-37.5	6.3	37.5-90	0.56	72
#T18412.050.072	800	400	1200	0.5	0.72	108	1995.1	30-37.5	15.5	45-90	0.73	82
#T18124.050.060	800	1200	400	0.5	0.6	59	2007.4	30-37.5	5.0	30-90	0.31	0
#T18124.050.065	800	1200	400	0.5	0.65	66	2012.6	30	6.4	22.5-90	0.49	0
#T18124.050.072	800	1200	400	0.5	0.72	72	2019.6	30-37.5	2.1	22.5-90	0.81	0
#T18124.050.075	800	1200	400	0.5	0.75	66	1995.1	30	2.1	37.5-90	0.50	0
#T181212.050.065	800	1200	1200	0.5	0.72	71	1996.9	30	6.1	37.5-90	0.63	0



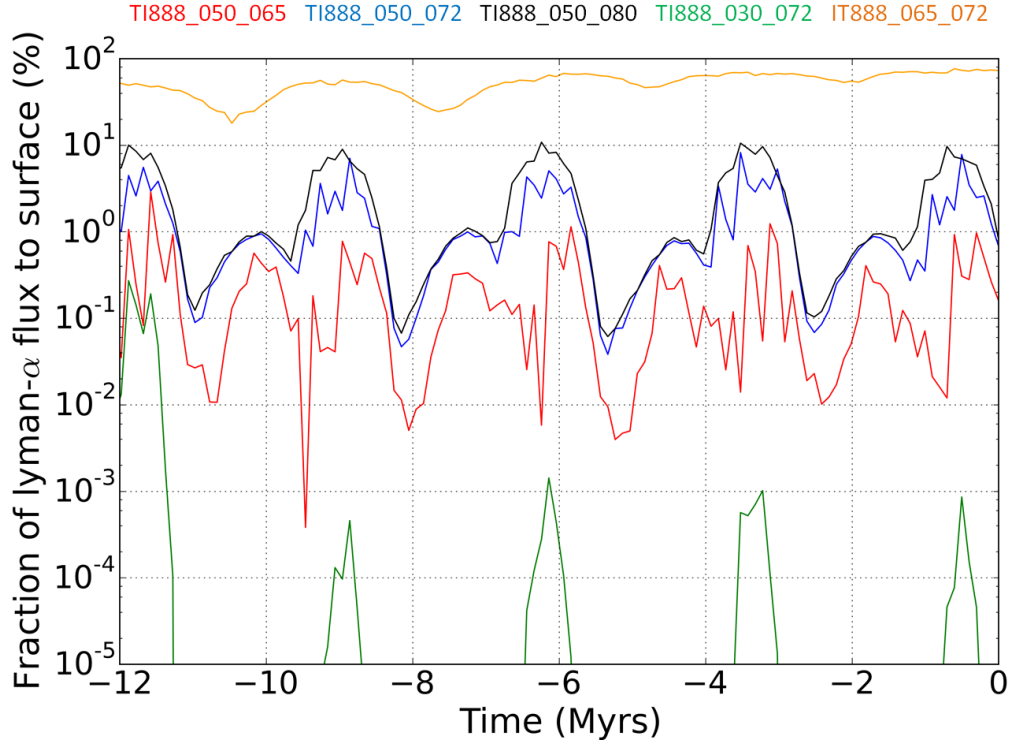


Fig. 17. Fraction of Lyman- $\alpha$  flux reaching Pluto's surface (on annual average) for the same simulations than on Figure 16.

## 5 Discussions

In this section, we first compare our results with Pluto's observations and further discuss the possible scenarios for the formation and evolution of the  $N_2$  and  $CH_4$  reservoirs.

### 5.1 Comparison of our results with Pluto's observations

#### 5.1.1 The massive equatorial $CH_4$ deposits

In our model,  $CH_4$  ice spontaneously tends to accumulate in the equatorial regions over astronomical timescales (see Section 3), forming thick perennial  $CH_4$  deposits. This explains the presence of the massive equatorial  $CH_4$ -rich Bladed Terrain Deposits observed by New Horizons (Moore et al., 2016, 2018; Earle et al., 2018b).

We obtain a slightly larger accumulation of  $CH_4$  ice north of the equator, which is consistent with the observed extension of the BTB, ranging in latitude from about 5°S to 28°N (see Fig. 4 in Earle et al., 2018b; Moore et al., 2018). This

location is reproduced by our simulations when assuming a medium-to-high soil thermal inertia (Figure 2). Similar results are obtained by starting the same simulation at another epoch. The equatorial deposits are also slightly more extended to the north if we start the simulation at  $t_0 = -100$  Myrs, but to the south if we start at  $t_0 = -200$  or  $-300$  Myrs, which are assumed to be different epochs with a perihelion occurring at northern fall or winter during maximum obliquity periods (Figure 5 in B2018).

Our results show that 30 Myrs is too short a period of time to form km-thick equatorial  $\text{CH}_4$ -rich deposits like the BTM. The BTM may be relatively old, as suggested by their dark albedo ( $\sim 0.5$ , Buratti et al. (2017)). The lack of craters suggests an upper limit on their age of 300 Myrs (Moore et al., 2018), although ancient craters may have been erased by intense sublimation of these terrains. We estimate that  $\sim 1$  km thick  $\text{CH}_4$ -rich deposits could form in the equatorial regions ( $30^\circ\text{S}$ - $30^\circ\text{N}$ ) over 50-100 Myrs, assuming an initial reservoir elsewhere (e.g. at the poles as in Section 3). Once this reservoir is depleted, extra hundreds of Myrs would be necessary to collect  $\text{CH}_4$  ice from the edges of the equatorial regions toward more equatorial latitudes and to pile up km-thick amounts of ice. If the BTM are only few hundreds meter thick, they could have formed over 50 Myrs or less.

In the model, the equatorial  $\text{CH}_4$  deposits form at all longitudes outside Sputnik Planitia. In reality, on Pluto, the unusual color of these terrains is only seen between longitudes  $210^\circ\text{E}$  to  $40^\circ\text{E}$  (Olkin et al., 2017; Moore et al., 2018; Earle et al., 2018b), and ground-based observations support the presence of more  $\text{CH}_4$ -rich deposits at these longitudes (Grundy and Buie, 2001; Grundy et al., 2013). This longitudinal asymmetry must be investigated with a full 3D Global Climate Model since it may be due to a dynamical effect of Pluto's atmosphere.

We also show in Section 4 that if the mid-to-polar  $\text{CH}_4$  deposits are bright enough (we evaluate the critical  $\text{CH}_4$  albedo around  $A_{\text{CH}_4}=0.6$ ), then mm-thick seasonal or meter-thick perennial  $\text{N}_2$  deposits can form in these regions, preferentially at low elevations. In this case, we find that the BTM are not stable and correspond to a net sublimation zone at the astronomical timescale, because  $\text{CH}_4$  ice is transferred from the BTM toward the mid-latitudes regions where it remains trapped by the perennial or seasonal  $\text{N}_2$  deposits. Assuming a  $\text{CH}_4$  albedo of 0.5 for the modeled BTM, we obtain a loss  $L_{\text{CH}_4} \sim 100$  m of ice over the 30 Myrs in most of our simulations (see Table 2). The km-thick BTM could therefore disappear within 300 Myrs.

These results suggest that the BTM were thicker in the past, and are now gradually disappearing. This is to be related to their bladed morphology, thought to be controlled by sublimation process (Moore et al., 2017; Moore et al., 2017, 2018).

### 5.1.2 *The perennial reservoirs of $N_2$ ice*

Our simulations show that, the closer to the equator, the more perennial are the  $N_2$  reservoirs (outside of Sputnik Planitia). As a general trend, our model simulates two types of perennial  $N_2$  reservoirs (apart from Sputnik Planitia). First, up to 200-300 m thick  $N_2$  ice deposits can form at the equator, at low elevations where relatively bright  $CH_4$  ice remains (albedo  $\sim 0.6$ ). This result is consistent with the detection of  $N_2$  ice in East Tombaugh Regio, in the depressions surrounding the BTM and in some deep craters in Cthulhu (e.g. Elliot crater, where evidences of polygonal cells may be supportive of a thick deposit), and suggests that these deposits may be stable over several Myrs. Second, a 10-20 m-thick mid-latitudinal band ( $30-45^\circ N$ ) of  $N_2$  ice forms in most of our simulations and remains over several Myrs, which is consistent with observations (see Fig. 15 in [Schmitt et al., 2017](#); [Protopapa et al., 2017](#)). The extent of such  $N_2$  ice deposits toward lower latitudes is limited by the presence of tholin-covered regions, which tend to darken the surrounding areas thus preventing further accumulation of volatile ice.

All  $N_2$  ice deposits are balanced by the main reservoir in Sputnik Planitia: as they form, the reservoir and therefore the surface level of  $N_2$  ice within the basin decreases which reinforces the  $N_2$  condensation in the basin ([Bertrand and Forget, 2016](#)), thus limiting the amount of  $N_2$  ice that can form elsewhere. We also note that  $CH_4$ -rich ice on Pluto may not be trapped and buried by very large  $N_2$ -rich deposits, since  $N_2$  ice is twice as dense as that of  $CH_4$  and may sink through the  $CH_4$  ice. For instance, on Triton, the Cantaloupe terrain may result from such a process ([Schenk and Jackson, 1993](#)).

### 5.1.3 *The mid-to-polar $N_2$ and $CH_4$ deposits*

At the north pole, New Horizons detected  $CH_4$ -rich deposits ([Grundy et al., 2016](#); [Schmitt et al., 2017](#); [Protopapa et al., 2017](#)). Most of our simulations reproduce this trend by predicting a seasonal (mm-thick)  $CH_4$  ice deposit exposed on Pluto's surface at the north pole in 2015 (e.g. Figure 5, Figure 11), quickly disappearing and revealing the dark volatile-free surface during the following years. However, such a thin deposit should have allowed the spectrometers on-board New Horizons for the detection of the water ice bedrock below. The fact that water ice has not been detected anywhere in the polar region strongly suggests that at least several centimeters or even meters of  $CH_4$ -rich ice cover this region (or else the water ice is buried under photolytic byproducts).

Simulations #TI888.030\_072 and #TI888.050\_080 (Figure 6 and Figure 8 respectively) show that such perennial  $CH_4$ -rich deposits can be obtained at the poles, by assuming a very dark albedo for the BTM or a very bright albedo

for the polar  $\text{CH}_4$  deposits. These results may be related to the yellow aspect of the polar region in false-color images (Olkin et al., 2017). For instance, the color may be due to the presence of tholins mixed with (or seen through) the thin  $\text{CH}_4$ -rich frost (Grundy et al., 2018). Alternatively, the polar reservoir of  $\text{CH}_4$  may be perennial and have accumulated tholins over the last Myrs. The higher concentration of tholins in these deposits may be responsible for their peculiar color.

At northern mid-latitudes, we obtain the formation of  $\text{N}_2$  ice deposits (on the bright  $\text{CH}_4$  deposits), which tend to be seasonal above  $37^\circ\text{N}$  as they sublime from the poles during end spring/summer. This result explains the mid-latitudinal band of  $\text{N}_2$ -rich ice observed in 2015 (Protopapa et al., 2017; Schmitt et al., 2017), and is consistent with the latitudinal distribution of the different ice mixtures observed at these latitudes, indicative of  $\text{N}_2$ :CO sublimation processes (Protopapa et al., 2017; Schmitt et al., 2017). Our results predict that  $\text{N}_2$  ice sublimation will continue during northern spring/summer (with a sublimation front advancing southward, as suggested in Protopapa et al. (2017)) and reveal more  $\text{CH}_4$ -rich terrains, while the redeposition of  $\text{N}_2$  ice will occur in the southern winter hemisphere. Note that  $\text{N}_2$  ice is always more stable in the depressions than outside, which explains the patchy distribution of  $\text{N}_2$  found at northern mid-latitudes (see Fig. 15 in Schmitt et al., 2017).

In the model, the seasonal mid-latitudinal  $\text{N}_2$  ice deposits are able to trap large amounts of  $\text{CH}_4$  ice, provided that a constant source is present elsewhere (in this case, the BTM). This also occurs in simulations performed at other epochs ( $t_0 = -100, -200, -300$  Myrs) and explains the thick mantle of ice observed by New Horizons at these latitudes.

In the model, the  $\text{N}_2$  ice deposits forming between  $30^\circ\text{N}$ - $37^\circ\text{N}$  tend to be perennial, because they are located in colder regions on average over several Myrs (this is an effect of subsurface thermal inertia, as shown by Fig. 4.b in B2018). At lower latitudes, the dark albedo of the equatorial volatile-free surface prevent further  $\text{N}_2$  condensation. However, thin  $\text{CH}_4$  frosts may form on these dark terrains during winter (see e.g Figure 11). This is consistent with the third latitudinal band observed on Pluto and mentioned in Protopapa et al. (2017), where  $\text{CH}_4$ -rich deposits are observed between  $20^\circ\text{N}$ - $30^\circ\text{N}$  (also shown in Earle et al., 2018b). At these latitudes, which border the dark tholin-covered regions,  $\text{N}_2$  ice deposits are not stable due to the darker albedo and the high rate of contamination and darkening by tholins. However,  $\text{CH}_4$ -rich frosts may form and last until spring/summer or even last longer and form perennial deposits.

Note that the exact latitudes where the volatile ice deposits form in the model are sensitive to the surface properties (albedo, emissivity, thermal inertia).

In addition, dilution and mixing processes of these ices should impact their latitudinal distribution.

#### 5.1.4 *Best case simulations*

A simulation that best matches Pluto’s observation would show (1) an ice distribution in 2015 as observed by New Horizons, that is with CH<sub>4</sub> ice exposed at the north pole and N<sub>2</sub> ice subliming at mid-latitudes, (2) a peak surface pressure occurring after 2015, and (3) an atmospheric mixing ratio for CH<sub>4</sub> around 0.5% in the period 2010-2015 (Lellouch et al., 2011a, 2015). In this paper, although we explored many cases and obtained a plethora of results, it is difficult to find one simulation that reconciles all these observations. Generally speaking, simulations performed with a thermal inertia for water ice of 400 SI give the best results. This thermal inertia is low compared to the estimations (Leyrat et al., 2016) but allows for thicker deposits of CH<sub>4</sub> at the poles, which is consistent with the observations.

### 5.2 *Scenario for the formation of observed CH<sub>4</sub>-rich and N<sub>2</sub>-rich reservoirs*

We have identified two perennial reservoirs of volatile ice on Pluto which add to Sputnik Planitia, as shown in Figure 18: the mid-latitudinal regions (mantle of CH<sub>4</sub> ice and meter-thick N<sub>2</sub> ice deposits) and the equatorial regions east of Sputnik Planitia (BTD of CH<sub>4</sub> ice and low-altitude N<sub>2</sub> ice deposits).

Our model is able to reproduce the formation of the equatorial and mid-latitudinal perennial CH<sub>4</sub> reservoirs, although not at the same time. Indeed, both the BTD and the mid-latitudinal CH<sub>4</sub> mantle need a source of available CH<sub>4</sub> ice to form, and in our simulations one reservoir dominates the other, depending on the assumed CH<sub>4</sub> albedo. This suggests a complex history for the formation of these perennial reservoirs.

The reservoir in Sputnik Planitia must have been the first to form, since the basin is the oldest geologic feature identified on Pluto (Moore et al., 2016, > 4 billion years), and since its infilling with all available surface N<sub>2</sub> ice has been modeled and estimated to be complete by tens of millions of years following its formation (Bertrand et al., 2018).

We could imagine that at a time in Pluto’s history, large CH<sub>4</sub>-rich ice deposits formed at the equator. At first, they may have been covered by N<sub>2</sub>-rich ice deposits, but as they thickened up and reached higher altitudes with time, N<sub>2</sub>-rich ice probably became less stable on these deposits and remained in depressions only. The high-altitude CH<sub>4</sub> ice deposits may have then become older and darker with time, forming a plateau of darkened CH<sub>4</sub>-rich, precursor

to the BTM. In our simulations, we show that there is a net transport of  $\text{CH}_4$  ice from the BTM to the mid-latitudes, suggesting that the thick mantle of  $\text{CH}_4$  ice is subsequent to the BTM, which could have formed by erosion and sublimation. Consequently, if the BTM formed very early in Pluto's history, why have they not entirely disappeared by now? One solution is that the current BTM formed only recently in Pluto's history, and may be currently disappearing. One could imagine that the astronomical cycles of Pluto may have changed over the last billion years and created the conditions for the BTM only recently. However, Pluto is thought to be subject to very little perturbations (Dobrovolskis et al., 1997) and the presence of non-eroded ancient craters at the equator demonstrates a certain stability of the astronomical cycles (Binzel et al., 2017). Another solution is that a long-term cycle exists between the perennial reservoirs, as illustrated by the black arrows on Figure 18. In this case, processes not taken into account in our model must exist and refill Pluto's system with  $\text{CH}_4$  gas and ice.

For instance, large amounts of  $\text{CH}_4$  could be released at the northern and southern edges of the Sputnik Planitia ice sheet during the high obliquity periods, where intense  $\text{N}_2$  sublimation occurs (Bertrand et al., 2018). In fact, New Horizons observations of the northern edge of the ice sheet revealed very dark plains of  $\text{N}_2$ -rich ice enriched in  $\text{CH}_4$  ice (1-2%, compared to 0.3% in the rest of the ice sheet), which supports this scenario (Protopapa et al., 2017).

Albedo and topography run-away variations may also play a significant role in redistributing  $\text{N}_2$  and  $\text{CH}_4$  ice to different reservoirs (Earle et al., 2018a), as well as changes in ice composition, saturation, contamination or irradiation (Schmitt et al., 2017; Protopapa et al., 2017; Grundy et al., 2018). Another possibility is the re-supply of large amounts of  $\text{CH}_4$  from Pluto's interior, where sources of  $\text{CH}_4$  clathrate could be stored and released over time via outgassing or cryovolcanism, as proposed on Titan (Lunine and Atreya, 2008; Moore et al., 2016).

The lack of knowledge about these mechanisms makes it difficult to infer the total  $\text{CH}_4$  inventory in the system. A lower limit could be estimated by assuming that the high latitudes are only covered by thin layers of  $\text{CH}_4$  ice and that most of the  $\text{CH}_4$  reservoir is contained in the Bladed Terrain Deposits (the contribution of 0.3-0.5% of  $\text{CH}_4$  in the  $\text{N}_2$  reservoir of Sputnik Planitia is negligible). Such a reservoir has been estimated to 22 m on global average in Section 2.4, for 500 m thick BTM, but could be raised to 100 m if we assume 2-2.5 km thick BTM. An upper limit of 1 km could be estimated by considering the BTM and a 1-km thick  $\text{CH}_4$  mantle at latitudes higher than  $15^\circ$  (740 m on global average). Note that the weak escape rate of  $\text{CH}_4$  observed by New Horizons suggests that the reservoir of  $\text{CH}_4$  changed by only 28 m over the age of the solar system (Gladstone et al., 2016).

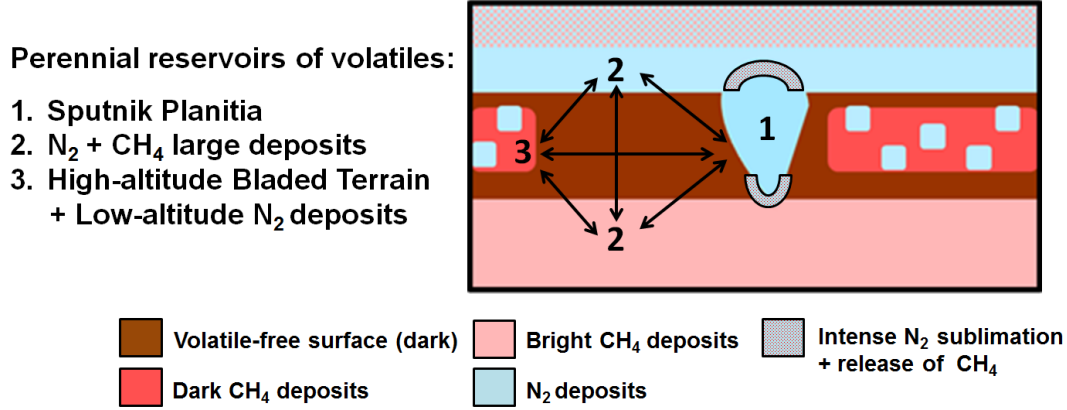


Fig. 18. The perennial reservoirs of  $\text{N}_2$  and  $\text{CH}_4$  ice identified on Pluto. The black arrows represent the possible exchanges of volatile ice that may occur over timescales of millions of years.

## 6 Conclusions

The Pluto volatile transport model has been used to simulate the evolution of large  $\text{N}_2$  and  $\text{CH}_4$  ice reservoirs over seasonal and astronomical timescales, in response to the Milankovitch paleoclimate cycles. This complements the work done by B2018, which only explored the cycles of  $\text{N}_2$ .

Our simulations reproduce the formation of massive perennial deposits of  $\text{CH}_4$ -rich ice at the equator, explaining the observation of the Bladed Terrain Deposits at these locations. The configuration of Pluto's orbit and obliquity is responsible for the small but detectable asymmetry of these terrains around the equator, which form further in the north than in the south, as seen in our model.

We demonstrate that high  $\text{CH}_4$  ice albedo values may sufficiently cool the surface and trigger  $\text{N}_2$  condensation which then cold traps more  $\text{CH}_4$  ice. We obtained a plethora of results depending on the assumed albedo for  $\text{CH}_4$  ice, which controls the perennial or seasonal nature of the deposits. Assuming relatively dark Bladed Terrain Deposits allows the formation of perennial  $\text{N}_2$  ice in the depressions of these terrains only, which is consistent with the observations. Assuming relatively bright mid-to-polar  $\text{CH}_4$  ice deposits leads to the formation of up to 10-m thick  $\text{N}_2$  deposits on the  $\text{CH}_4$  ice deposits, in particular at low elevations. During northern spring and summer, these  $\text{N}_2$  deposits sublime from the pole, explaining the latitudinal distribution of  $\text{N}_2$ -rich and  $\text{CH}_4$ -rich ices observed by New Horizons in 2015 at the mid-northern latitudes (Protopapa et al., 2017; Schmitt et al., 2017).

At the north pole, the disappearance of  $\text{CH}_4$ -rich frost during the next decade predicted by most of our simulation may not happen because the observations



suggest larger deposits than those simulated. However, this is a testable prediction, as well as the removal of  $\text{N}_2$ -rich ice from the northern high latitudes, since it should result in changes in Pluto’s spectrum and maybe albedo and color, observable from Earth.

Our simulations also show that a large amount of  $\text{CH}_4$  ice can accumulate in the mid-latitudes due to the cold-trap effect of  $\text{N}_2$  ice, forming a thick mantle consistent with the observations of Pluto’s surface by New Horizons. In the model,  $\text{CH}_4$  ice is moved from the Bladed Terrain Deposits, which tends to disappear as the mid-latitude mantle forms.

These simulations indicate that there is always enough gaseous  $\text{CH}_4$  in Pluto’s atmosphere for it to remain relatively opaque at Lyman- $\alpha$  wavelengths over astronomical cycles, in particular during high-to-moderate obliquity periods. However, the small amounts of Lyman- $\alpha$  flux reaching the surface can be significant to the surface chemistry.

Finally, our results highlight the strong coupling between the  $\text{CH}_4$  and the  $\text{N}_2$  cycle and the role of  $\text{CH}_4$  material as a controlling agent of this coupling. They suggest a complex history for Pluto’s perennial reservoirs as large amounts of  $\text{CH}_4$  ice may have been exchanged between Sputnik Planitia, the Bladed Terrain, and the mid-latitudes, over timescales of hundreds of million years. The evolution of these reservoirs may be driven by positive (“run-away”) or negative feedbacks involving ice albedo, emissivity, dilution and mixing coefficient, contamination by haze particles, or ice irradiation. In order to improve our understanding of Pluto’s surface, future versions of the Pluto volatile transport model should implement these processes and explore how they impact Pluto’s climate.



## References

- T. Bertrand and F. Forget. 3D modeling of organic haze in Pluto's atmosphere. *Icarus*, 287:72–86, May 2017. doi: 10.1016/j.icarus.2017.01.016.
- T. Bertrand and F. Forget. Observed glacier and volatile distribution on Pluto from atmospheretopography processes. *Nature*, 987, December 2016. doi: 10.1038/nature19337.
- T. Bertrand, F. Forget, O. M. Umurhan, W. M. Grundy, B. Schmitt, S. Protopapa, A. M. Zangari, O. L. White, P. M. Schenk, K. N. Singer, A. Stern, H. A. Weaver, L. A. Young, K. Ennico, and C. B. Olkin. The nitrogen cycles on Pluto over seasonal and astronomical timescales. *Icarus*, 309:277–296, July 2018. doi: 10.1016/j.icarus.2018.03.012.
- R. P. Binzel, A. M. Earle, M. W. Buie, L. A. Young, S. A. Stern, C. B. Olkin, K. Ennico, J. M. Moore, W. Grundy, H. A. Weaver, C. M. Lisse, and T. R. Lauer. Climate zones on Pluto and Charon. *Icarus*, 287:30–36, May 2017. doi: 10.1016/j.icarus.2016.07.023.
- B. J. Buratti, J. D. Hofgartner, M. D. Hicks, H. A. Weaver, S. A. Stern, T. Momary, J. A. Mosher, R. A. Beyer, A. J. Verbiscer, A. M. Zangari, L. A. Young, C. M. Lisse, K. Singer, A. Cheng, W. Grundy, K. Ennico, and C. B. Olkin. Global albedos of Pluto and Charon from LORRI New Horizons observations. *Icarus*, 287:207–217, May 2017. doi: 10.1016/j.icarus.2016.11.012.
- A. R. Dobrovolskis, S. J. Peale, and A. W. Harris. *Dynamics of the Pluto-Charon Binary*. In: S.A. Stern, D.J. Tholen (Eds.), *Pluto and Charon*, University of Arizona Press, Tucson, 159-190. 1997.
- A. M. Earle, R. P. Binzel, L. A. Young, S. A. Stern, K. Ennico, W. Grundy, C. B. Olkin, and H. A. Weaver. Long-term surface temperature modeling of Pluto. *Icarus*, 287:37–46, May 2017. doi: 10.1016/j.icarus.2016.09.036.
- A. M. Earle, R. P. Binzel, L. A. Young, S. A. Stern, K. Ennico, W. Grundy, C. B. Olkin, H. A. Weaver, and New Horizons Surface Composition Theme. Albedo matters: Understanding runaway albedo variations on Pluto. *Icarus*, 303:1–9, March 2018a. doi: 10.1016/j.icarus.2017.12.015.
- A. M. Earle, W. Grundy, C. J. A. Howett, C. B. Olkin, A. H. Parker, F. Scipioni, R. P. Binzel, R. A. Beyer, J. C. Cook, D. P. Cruikshank, C. M. Dalle Ore, K. Ennico, S. Protopapa, D. C. Reuter, P. M. Schenk, B. Schmitt, S. A. Stern, H. A. Weaver, L. A. Young, and New Horizons Surface Composition Theme Team. Methane distribution on Pluto as mapped by the New Horizons Ralph/MVIC instrument. *Icarus*, 314:195–209, November 2018b. doi: 10.1016/j.icarus.2018.06.005.
- J. Eluszkiewicz and D. J. Stevenson. Rheology of solid methane and nitrogen - Applications of Triton. *Geophys. Res. Lett.*, 17:1753–1756, September 1990. doi: 10.1029/GL017i010p01753.
- F. Forget, T. Bertrand, M. Vangvichith, J. Leconte, E. Millour, and E. Lellouch. A post-new horizons global climate model of Pluto including the N<sub>2</sub>, CH<sub>4</sub> and CO cycles. *Icarus*, 287:54–71, May 2017. doi: 10.1016/j.icarus.

2016.11.038.

- G. Gladstone, W. R. Pryor, and S. Alan Stern. Ly  $\alpha$  @Pluto. *Icarus*, 246: 279–284, January 2015. doi: 10.1016/j.icarus.2014.04.016.
- G. R. Gladstone, S. A. Stern, K. Ennico, C. B. Olkin, H. A. Weaver, L. A. Young, M. E. Summers, D. F. Strobel, D. P. Hinson, J. A. Kammer, A. H. Parker, A. J. Steffl, I. R. Linscott, J. W. Parker, A. F. Cheng, D. C. Slater, M. H. Versteeg, T. K. Greathouse, K. D. Retherford, H. Throop, N. J. Cunningham, W. W. Woods, K. N. Singer, C. C. C. Tsang, E. Schindhelm, C. M. Lisse, M. L. Wong, Y. L. Yung, X. Zhu, W. Curdt, P. Lavvas, E. F. Young, G. L. Tyler, F. Bagenal, W. M. Grundy, W. B. McKinnon, J. M. Moore, J. R. Spencer, T. Andert, J. Andrews, M. Banks, B. Bauer, J. Bauman, O. S. Barnouin, P. Bedini, K. Beisser, R. A. Beyer, S. Bhaskaran, R. P. Binzel, E. Birath, M. Bird, D. J. Bogan, A. Bowman, V. J. Bray, M. Brozovic, C. Bryan, M. R. Buckley, M. W. Buie, B. J. Buratti, S. S. Bushman, A. Calloway, B. Carcich, S. Conard, C. A. Conrad, J. C. Cook, D. P. Cruikshank, O. S. Custodio, C. M. D. Ore, C. Deboy, Z. J. B. Dischner, P. Dumont, A. M. Earle, H. A. Elliott, J. Ercol, C. M. Ernst, T. Finley, S. H. Flanigan, G. Fountain, M. J. Freeze, J. L. Green, Y. Guo, M. Hahn, D. P. Hamilton, S. A. Hamilton, J. Hanley, A. Harch, H. M. Hart, C. B. Hersman, A. Hill, M. E. Hill, M. E. Holdridge, M. Horanyi, A. D. Howard, C. J. A. Howett, C. Jackman, R. A. Jacobson, D. E. Jennings, H. K. Kang, D. E. Kaufmann, P. Kollmann, S. M. Krimigis, D. Kusnierkiewicz, T. R. Lauer, J. E. Lee, K. L. Lindstrom, A. W. Lunsford, V. A. Mallder, N. Martin, D. J. McComas, R. L. McNutt, D. Mehoke, T. Mehoke, E. D. Melin, M. Mutchler, D. Nelson, F. Nimmo, J. I. Nunez, A. Ocampo, W. M. Owen, M. Paetzold, B. Page, F. Pelletier, J. Peterson, N. Pinkine, M. Piquette, S. B. Porter, S. Protopapa, J. Redfern, H. J. Reitsema, D. C. Reuter, J. H. Roberts, S. J. Robbins, G. Rogers, D. Rose, K. Runyon, M. G. Ryschkewitsch, P. Schenk, B. Sepan, M. R. Showalter, M. Soluri, D. Stanbridge, T. Stryk, J. R. Szalay, M. Tapley, A. Taylor, H. Taylor, O. M. Umurhan, A. J. Verbiscer, M. H. Versteeg, M. Vincent, R. Webbert, S. Weidner, G. E. Weigle, O. L. White, K. Whittenburg, B. G. Williams, K. Williams, S. Williams, A. M. Zangari, and E. Zirnstien. The atmosphere of Pluto as observed by New Horizons. *Science*, 351:aad8866, March 2016. doi: 10.1126/science.aad8866.
- W. M. Grundy and M. W. Buie. Distribution and Evolution of CH<sub>4</sub>, N<sub>2</sub>, and CO Ices on Pluto’s Surface: 1995 to 1998. *Icarus*, 153:248–263, October 2001. doi: 10.1006/icar.2001.6684.
- W. M. Grundy, C. B. Olkin, L. A. Young, M. W. Buie, and E. F. Young. Near-infrared spectral monitoring of Pluto’s ices: Spatial distribution and secular evolution. *Icarus*, 223:710–721, April 2013. doi: 10.1016/j.icarus.2013.01.019.
- W. M. Grundy, R. P. Binzel, B. J. Buratti, J. C. Cook, D. P. Cruikshank, C. M. Dalle Ore, A. M. Earle, K. Ennico, C. J. A. Howett, A. W. Lunsford, C. B. Olkin, A. H. Parker, S. Philippe, S. Protopapa, E. Quirico, D. C. Reuter, B. Schmitt, K. N. Singer, A. J. Verbiscer, R. A. Beyer, M. W. Buie,

- A. F. Cheng, D. E. Jennings, I. R. Linscott, J. W. Parker, P. M. Schenk, J. R. Spencer, J. A. Stansberry, S. A. Stern, H. B. Throop, C. C. C. Tsang, H. A. Weaver, G. E. Weigle, and L. A. Young. Surface compositions across Pluto and Charon. *Science*, 351:aad9189, March 2016. doi: 10.1126/science.aad9189.
- W. M. Grundy, T. Bertrand, R. P. Binzel, M. W. Buie, B. J. Buratti, A. F. Cheng, J. C. Cook, D. P. Cruikshank, S. L. Devins, C. M. Dalle Ore, A. M. Earle, K. Ennico, F. Forget, P. Gao, G. R. Gladstone, C. J. A. Howett, D. E. Jennings, J. A. Kammer, T. R. Lauer, I. R. Linscott, C. M. Lisse, A. W. Lunsford, W. B. McKinnon, C. B. Olkin, A. H. Parker, S. Protopapa, E. Quirico, D. C. Reuter, B. Schmitt, K. N. Singer, J. A. Spencer, S. A. Stern, D. F. Strobel, M. E. Summers, H. A. Weaver, G. E. Weigle, M. L. Wong, E. F. Young, L. A. Young, and X. Zhang. Pluto’s haze as a surface material. *Icarus*, 314:232–245, November 2018. doi: 10.1016/j.icarus.2018.05.019.
- C. J. Hansen and D. A. Paige. Seasonal Nitrogen Cycles on Pluto. *Icarus*, 120:247–265, April 1996. doi: 10.1006/icar.1996.0049.
- C. J. Hansen, D. A. Paige, and L. A. Young. Pluto’s climate modeled with new observational constraints. *Icarus*, 246:183–191, January 2015. doi: 10.1016/j.icarus.2014.03.014.
- A. D. Howard, J. M. Moore, O. M. Umurhan, O. L. White, R. S. Anderson, W. B. McKinnon, J. R. Spencer, P. M. Schenk, R. A. Beyer, S. A. Stern, K. Ennico, C. B. Olkin, H. A. Weaver, and L. A. Young. Present and past glaciation on Pluto. *Icarus*, 287:287–300, May 2017. doi: 10.1016/j.icarus.2016.07.006.
- E. Lellouch, C. de Bergh, B. Sicardy, H. U. Käufl, and A. Smette. High resolution spectroscopy of Pluto’s atmosphere: detection of the  $2.3\ \mu\text{m}$   $\text{CH}_4$  bands and evidence for carbon monoxide. *Astronomy & Astroph.*, 530:L4, June 2011a. doi: 10.1051/0004-6361/201116954.
- E. Lellouch, J. Stansberry, J. Emery, W. Grundy, and D. P. Cruikshank. Thermal properties of Pluto’s and Charon’s surfaces from Spitzer observations. *Icarus*, 214:701–716, August 2011b. doi: 10.1016/j.icarus.2011.05.035.
- E. Lellouch, C. de Bergh, B. Sicardy, F. Forget, M. Vangvichith, and H.-U. Käufl. Exploring the spatial, temporal, and vertical distribution of methane in Pluto’s atmosphere. *Icarus*, 246:268–278, January 2015. doi: 10.1016/j.icarus.2014.03.027.
- C. Leyrat, R. D. Lorenz, and A. Le Gall. Probing Pluto’s underworld: Ice temperatures from microwave radiometry decoupled from surface conditions. *Icarus*, 268:50–55, April 2016. doi: 10.1016/j.icarus.2015.12.016.
- J. Lunine and S. Atreya. The methane cycle on Titan. *Nature Geoscience*, 1: 335, May 2008. doi: 10.1038/ngeo187.
- C. K. Materese, D. P. Cruikshank, S. A. Sandford, H. Imanaka, and M. Nuevo. Ice Chemistry on Outer Solar System Bodies: Electron Radiolysis of  $\text{N}_2$ -,  $\text{CH}_4$ -, and  $\text{CO}$ -Containing Ices. *Astrophys. J.*, 812:150, October 2015. doi: 10.1088/0004-637X/812/2/150.

- F. Merlin. New constraints on the surface of Pluto. *Astronomy&Astroph.*, 582:A39, October 2015. doi: 10.1051/0004-6361/201526721.
- J. M. Moore, W. B. McKinnon, J. R. Spencer, A. D. Howard, P. M. Schenk, R. A. Beyer, F. Nimmo, K. N. Singer, O. M. Umurhan, O. L. White, S. A. Stern, K. Ennico, C. B. Olkin, H. A. Weaver, L. A. Young, R. P. Binzel, M. W. Buie, B. J. Buratti, A. F. Cheng, D. P. Cruikshank, W. M. Grundy, I. R. Linscott, H. J. Reitsema, D. C. Reuter, M. R. Showalter, V. J. Bray, C. L. Chavez, C. J. A. Howett, T. R. Lauer, C. M. Lisse, A. H. Parker, S. B. Porter, S. J. Robbins, K. Runyon, T. Stryk, H. B. Throop, C. C. C. Tsang, A. J. Verbiscer, A. M. Zangari, A. L. Chaikin, D. E. Wilhelms, F. Bagenal, G. R. Gladstone, T. Andert, J. Andrews, M. Banks, B. Bauer, J. Bauman, O. S. Barnouin, P. Bedini, K. Beisser, S. Bhaskaran, E. Birath, M. Bird, D. J. Bogan, A. Bowman, M. Brozovic, C. Bryan, M. R. Buckley, S. S. Bushman, A. Calloway, B. Carcich, S. Conard, C. A. Conrad, J. C. Cook, O. S. Custodio, C. M. D. Ore, C. Deboy, Z. J. B. Dischner, P. Dumont, A. M. Earle, H. A. Elliott, J. Ercol, C. M. Ernst, T. Finley, S. H. Flanigan, G. Fountain, M. J. Freeze, T. Greathouse, J. L. Green, Y. Guo, M. Hahn, D. P. Hamilton, S. A. Hamilton, J. Hanley, A. Harch, H. M. Hart, C. B. Hersman, A. Hill, M. E. Hill, D. P. Hinson, M. E. Holdridge, M. Horanyi, C. Jackman, R. A. Jacobson, D. E. Jennings, J. A. Kammer, H. K. Kang, D. E. Kaufmann, P. Kollmann, S. M. Krimigis, D. Kusnierkiewicz, J. E. Lee, K. L. Lindstrom, A. W. Lunsford, V. A. Mallder, N. Martin, D. J. McComas, R. L. McNutt, D. Mehoke, T. Mehoke, E. D. Melin, M. Mutchler, D. Nelson, J. I. Nunez, A. Ocampo, W. M. Owen, M. Paetzold, B. Page, J. W. Parker, F. Pelletier, J. Peterson, N. Pinkine, M. Piquette, S. Protopapa, J. Redfern, J. H. Roberts, G. Rogers, D. Rose, K. D. Retherford, M. G. Ryschkewitsch, E. Schindhelm, B. Sepan, M. Soluri, D. Stanbridge, A. J. Steffl, D. F. Strobel, M. E. Summers, J. R. Szalay, M. Tapley, A. Taylor, H. Taylor, G. L. Tyler, M. H. Versteeg, M. Vincent, R. Webbert, S. Weidner, G. E. Weigle, K. Whittenburg, B. G. Williams, K. Williams, S. Williams, W. W. Woods, and E. Zirnstein. The geology of Pluto and Charon through the eyes of New Horizons. *Science*, 351:1284–1293, March 2016. doi: 10.1126/science.aad7055.
- J. M. Moore, A. D. Howard, O. M. Umurhan, O. L. White, P. M. Schenk, R. A. Beyer, W. B. McKinnon, J. R. Spencer, W. M. Grundy, T. R. Lauer, F. Nimmo, L. A. Young, S. A. Stern, H. A. Weaver, C. B. Olkin, and K. Ennico. Sublimation as a landform-shaping process on Pluto. *Icarus*, 287: 320–333, May 2017. doi: 10.1016/j.icarus.2016.08.025.
- J. M. Moore, A. D. Howard, O. M. Umurhan, O. L. White, P. M. Schenk, R. A. Beyer, W. B. McKinnon, J. R. Spencer, K. N. Singer, W. M. Grundy, A. M. Earle, B. Schmitt, S. Protopapa, F. Nimmo, D. P. Cruikshank, D. P. Hinson, L. A. Young, S. A. Stern, H. A. Weaver, C. B. Olkin, K. Ennico, G. Collins, T. Bertrand, F. Forget, F. Scipioni, and New Horizons Science Team. Bladed Terrain on Pluto: Possible origins and evolution. *Icarus*, 300: 129–144, January 2018. doi: 10.1016/j.icarus.2017.08.031.

- J. E. Moores, C. L. Smith, A. D. Toigo, and S. D. Guzewich. Penitentes as the origin of the bladed terrain of Tartarus Dorsa on Pluto. *Nature*, 541: 188–190, January 2017. doi: 10.1038/nature20779.
- C. B. Olkin, L. A. Young, D. Borncamp, A. Pickles, B. Sicardy, M. Assafin, F. B. Bianco, M. W. Buie, A. D. de Oliveira, M. Gillon, R. G. French, A. Ramos Gomes, E. Jehin, N. Morales, C. Opitom, J. L. Ortiz, A. Maury, M. Norbury, F. Braga-Ribas, R. Smith, L. H. Wasserman, E. F. Young, M. Zacharias, and N. Zacharias. Evidence that Pluto’s atmosphere does not collapse from occultations including the 2013 May 04 event. *Icarus*, 246:220–225, January 2015. doi: 10.1016/j.icarus.2014.03.026.
- C. B. Olkin, J. R. Spencer, W. M. Grundy, A. H. Parker, R. A. Beyer, P. M. Schenk, C. J. A. Howett, S. A. Stern, D. C. Reuter, H. A. Weaver, L. A. Young, K. Ennico, R. P. Binzel, M. W. Buie, J. C. Cook, D. P. Cruikshank, C. M. Dalle Ore, A. M. Earle, D. E. Jennings, K. N. Singer, I. E. Linscott, A. W. Lunsford, S. Protopapa, B. Schmitt, E. Weigle, and the New Horizons Science Team. The Global Color of Pluto from New Horizons. *AJ*, 154:258, December 2017. doi: 10.3847/1538-3881/aa965b.
- S. Protopapa, W. M. Grundy, D. C. Reuter, D. P. Hamilton, C. M. Dalle Ore, J. C. Cook, D. P. Cruikshank, B. Schmitt, S. Philippe, E. Quirico, R. P. Binzel, A. M. Earle, K. Ennico, C. J. A. Howett, A. W. Lunsford, C. B. Olkin, A. Parker, K. N. Singer, A. Stern, A. J. Verbiscer, H. A. Weaver, and L. A. Young. Pluto’s global surface composition through pixel-by-pixel Hapke modeling of New Horizons Ralph/LEISA data. *Icarus*, 287:218–228, May 2017. doi: 10.1016/j.icarus.2016.11.028.
- P. Schenk and M. P. A. Jackson. Diapirism on Triton - A record of crustal layering and instability. *Geology*, 21:299–302, April 1993. doi: 10.1130/0091-7613(1993)021<0299:DOTARO>2.3.CO;2.
- B. Schmitt, S. Philippe, W. M. Grundy, D. C. Reuter, R. Cote, E. Quirico, S. Protopapa, L. A. Young, R. P. Binzel, J. C. Cook, D. P. Cruikshank, C. M. Dalle Ore, A. M. Earle, K. Ennico, C. J. A. Howett, D. E. Jennings, I. R. Linscott, A. W. Lunsford, C. B. Olkin, A. H. Parker, J. W. Parker, K. N. Singer, J. R. Spencer, J. A. Stansberry, S. A. Stern, C. C. C. Tsang, A. J. Verbiscer, and H. A. Weaver. Physical state and distribution of materials at the surface of Pluto from New Horizons LEISA imaging spectrometer. *Icarus*, 287:229–260, May 2017. doi: 10.1016/j.icarus.2016.12.025.
- J. R. Spencer, J. A. Stansberry, L. M. Trafton, E. F. Young, R. P. Binzel, and S. K. Croft. Volatile Transport, Seasonal Cycles, and Atmospheric Dynamics on Pluto. In S. A. Stern and D. J. Tholen, editors, *Pluto and Charon*, page 435, 1997.
- J. A. Stansberry and R. V. Yelle. Emissivity and the Fate of Pluto’s Atmosphere. *Icarus*, 141:299–306, October 1999. doi: 10.1006/icar.1999.6169.
- S. A. Stern, F. Bagenal, K. Ennico, G. R. Gladstone, W. M. Grundy, W. B. McKinnon, J. M. Moore, C. B. Olkin, J. R. Spencer, H. A. Weaver, L. A. Young, T. Andert, J. Andrews, M. Banks, B. Bauer, J. Bauman, O. S. Barnouin, P. Bedini, K. Beisser, R. A. Beyer, S. Bhaskaran, R. P. Binzel,

- E. Birath, M. Bird, D. J. Bogan, A. Bowman, V. J. Bray, M. Brozovic, C. Bryan, M. R. Buckley, M. W. Buie, B. J. Buratti, S. S. Bushman, A. Calloway, B. Carcich, A. F. Cheng, S. Conard, C. A. Conrad, J. C. Cook, D. P. Cruikshank, O. S. Custodio, C. M. Dalle Ore, C. Deboy, Z. J. B. Dischner, P. Dumont, A. M. Earle, H. A. Elliott, J. Ercol, C. M. Ernst, T. Finley, S. H. Flanigan, G. Fountain, M. J. Freeze, T. Greathouse, J. L. Green, Y. Guo, M. Hahn, D. P. Hamilton, S. A. Hamilton, J. Hanley, A. Harch, H. M. Hart, C. B. Hersman, A. Hill, M. E. Hill, D. P. Hinson, M. E. Holdridge, M. Horanyi, A. D. Howard, C. J. A. Howett, C. Jackman, R. A. Jacobson, D. E. Jennings, J. A. Kammer, H. K. Kang, D. E. Kaufmann, P. Kollmann, S. M. Krimigis, D. Kusnierkiewicz, T. R. Lauer, J. E. Lee, K. L. Lindstrom, I. R. Linscott, C. M. Lisse, A. W. Lunsford, V. A. Mallder, N. Martin, D. J. McComas, R. L. McNutt, D. Mehoke, T. Mehoke, E. D. Melin, M. Mutchler, D. Nelson, F. Nimmo, J. I. Nunez, A. Ocampo, W. M. Owen, M. Paetzold, B. Page, A. H. Parker, J. W. Parker, F. Pelletier, J. Peterson, N. Pinkine, M. Piquette, S. B. Porter, S. Protopapa, J. Redfern, H. J. Reitsema, D. C. Reuter, J. H. Roberts, S. J. Robbins, G. Rogers, D. Rose, K. Runyon, K. D. Retherford, M. G. Ryschkewitsch, P. Schenk, E. Schindhelm, B. Sepan, M. R. Showalter, K. N. Singer, M. Soluri, D. Stanbridge, A. J. Steffl, D. F. Strobel, T. Stryk, M. E. Summers, J. R. Szalay, M. Tapley, A. Taylor, H. Taylor, H. B. Throop, C. C. C. Tsang, G. L. Tyler, O. M. Umurhan, A. J. Verbiscer, M. H. Versteeg, M. Vincent, R. Webbert, S. Weidner, G. E. Weigle, O. L. White, K. Whittenburg, B. G. Williams, K. Williams, S. Williams, W. W. Woods, A. M. Zangari, and E. Zirnstein. The Pluto system: Initial results from its exploration by New Horizons. *Science*, 350:aad1815, October 2015. doi: 10.1126/science.aad1815.
- S. P. Tan and J. S. Kargel. Solid-phase equilibria on Pluto’s surface. *MNRAS*, 474:4254–4263, March 2018. doi: 10.1093/mnras/stx3036.
- A. D. Toigo, R. G. French, P. J. Gierasch, S. D. Guzewich, X. Zhu, and M. I. Richardson. General circulation models of the dynamics of Pluto’s volatile transport on the eve of the New Horizons encounter. *Icarus*, 254:306–323, July 2015. doi: 10.1016/j.icarus.2015.03.034.
- L. M. Trafton. On the state of methane and nitrogen ice on Pluto and Triton: Implications of the binary phase diagram. *Icarus*, 246:197–205, January 2015. doi: 10.1016/j.icarus.2014.05.022.
- E. F. Young. *An Albedo Map and Frost Model of Pluto*. PhD thesis, MASSACHUSETTS INSTITUTE OF TECHNOLOGY., 1993.
- L. A. Young. Pluto’s Seasons: New Predictions for New Horizons. *Astrophys. J.*, 766:L22, April 2013. doi: 10.1088/2041-8205/766/2/L22.
- L.A. Young. Volatile transport on inhomogeneous surfaces: I - analytic expressions, with application to pluto’s day. *Icarus*, 221:80–88, 2012.

## Acknowledgements

This work was supported by the CNES. It is based on observations of the New Horizons space mission. The authors thank the whole NASA *New Horizons* instrument and scientific team for their excellent work on a fantastic mission and their interest in this research. T. B. was supported for this research by an appointment to the National Aeronautics and Space Administration (NASA) Post-doctoral Program at the Ames Research Center administered by Universities Space Research Association (USRA) through a contract with NASA.